J. Fluid Mech. (1993), *vol.* 253, *pp.* 105–140

Coherent structures in oscillatory boundary layers

By TURGUT SARPKAYA
Naval Postgraduate School, Monterey, CA 93943, USA

(Received 5 June 1992 and in revised form 29 January 1993)

An experimental investigation of the circumstances leading to the creation and subsequent evolution of the low-speed streaks and other quasi-coherent structures on a long cylindrical body immersed in a sinusoidally oscillating flow (Stokes flow) is described. The wall shear stress and the phase lead of the maximum wall shear over the maximum free-stream velocity have been measured to characterize the unsteady boundary layer. The evolution of a sinuous streak, from its inception to its ultimate demise, and the generation of multiple streaks, arches, hairpins, and other vortical structures have been traced through flow visualization. The results have shown that the strong pressure gradients, inflexion points in the velocity profile, and the reversal of the shear stress have profound effects on the stability of the flow. The Reynolds number ($Re_\delta = U_{\max}\,\delta/\nu$) delineates the boundaries of the laminar stable flow, transitional flow, and turbulent flow at the start of which the phase angle decreases sharply, the friction coefficient increases rapidly, and the turbulent motion prevails over larger fractions of the flow cycle. The transitional and turbulent states are rich with vortical motions which burst themselves into existence most intensely during the later stages of the deceleration phase. The effect of the manipulation of the viscosity of the wall-layer fluid on the creation and bifurcation of the low-speed streaks is discussed in some detail.

1. Introduction

The primary aim of the present investigation is to examine, through the use of laser-induced fluorescence (LIF), the inception and response of low-speed streaks and other turbulence structures to periodic accelerations and decelerations of an oscillatory Stokes flow along a cylinder of sufficiently large radius with the hope of elucidating the causality and mechanisms of transition to turbulence. It is hoped that the cyclic nature of the unbounded flow over a hydrodynamically 'plane' smooth surface will provide a better opportunity to observe the evolution of the various types of quasi-coherent structures, from their incipient existence to their ultimate demise. A concomitant objective of the investigation is to provide shear force and phase data to establish the character of the oscillatory flow used.

1.1. *Low-speed streaks and other structures*

Much has been contributed towards the understanding of the structure of canonical turbulent wall flows (pipe, channel and boundary layer without a pressure gradient) over large ranges of Reynolds number through analytical and numerical studies, hot-wire measurements, and flow visualization (e.g. Kline *et al.* 1967; Corino & Brodkey 1969; Kim, Kline & Reynolds 1971; Nychas, Hershey & Brodkey 1973; Blackwelder & Eckelmann 1979; Head & Bandyopadhyay 1981; Kim & Moin 1986; Landahl 1990; Robinson 1991; Smith *et al.* 1991; Jimenez & Moin 1991; Lam & Banerjee 1992). For incisive as well as eloquent reviews of the state of the art, deduced from forty years of experimentation and ten years of numerical simulation of low-Reynolds-number

canonical flows, the reader is referred to Robinson & Kline (1990); Smith *et al.* (1991) and Robinson (1991).

The low-speed streaks and quasi-coherent vortical structures are now considered to be ubiquitous features of a turbulent boundary layer near a solid wall. The understanding of their origin and interaction with their surroundings holds the key to the dynamic modelling and the control of the consequences of turbulence on heat, mass, and momentum transfer. It is not yet clear as to why the formation of streaks, their lift off, oscillation, instability, and breakdown, followed by an in-sweep of faster moving fluid toward the wall are nature's preferred mechanisms of extracting vorticity in quasi-coherent quanta from a solid boundary. It appears that a unified view of the turbulence production cycle (the Holy Grail of turbulence) has not yet been found.

The use of steady ambient flow helps one to observe and sample the interactions of low-speed streaks, streamwise vorticity, arches, hairpin vortices, and near-wall shear layers, at different frequencies, over an arbitrary time interval. However, without a clear beginning or a clear end, unimpeded by a large number of mutually interacting, coalescing, and reconnecting vortex elements in the midst of background disturbances, the cause-and-effect relationships often become intermingled and elusive. Notwithstanding the desire to understand the low-speed streaks and the bursting phenomenon in steady boundary layers, it is believed that the observation of the birth, evolution, and self-replication of the vortical structures in non-canonical flows (e.g. an oscillatory Stokes flow) may provide one with additional physical insight, as well as additional questions, regarding the origins and dynamical features of the transition and turbulence. Some events may be common to all flows and some others may be unique to a particular flow situation. For an oscillatory Stokes flow, for example, the laminar flow is self-similar, inflexion points occur naturally, at least during part of the cycle, the oscillatory-flow structures exhibit time dependence that is phase locked with the deceleration part of the cycle, as noted by previous investigators (e.g. Fishler & Brodkey 1991), relaminarization may take place during some parts of the acceleration period, and the recycling of the flow structures to the region of their original creation may give rise to new events and complex history effects. Thus, the discovery of the common flow features may be more illuminating than the discovery of case-specific events and structures.

1.2. *Oscillatory Stokes flow*

Stokes provided the first theoretical solution of the motion of unbounded fluid over an infinite flat plate executing sinusoidal oscillations ($U = U_{\max} \sin \omega t$) along its plane (known as Stokes' second problem). Since then, considerable research has been carried out on oscillatory flow (with zero mean), and pulsatile flow (with non-zero mean) in pipes and over flat plates, including progressive water waves over rigid or mobile bottoms, through the use of velocity and turbulence measurements, flow visualization, and force measurements (for pulsatile flow, see e.g. Lighthill 1954; Sarpkaya 1966; Cousteix, Houdeville & Javelle 1981; Ramaprian & Tu 1983; Tardu, Binder & Blackwelder 1987; Mankbadi & Liu 1992; for oscillatory flow, see e.g. Li 1954; Collins 1963; Sergeev 1966; Merkli & Thomann 1975; Hino *et al.* 1976, 1983; von Kerczek & Davis 1974; Kamphuis 1975; Hall 1978; Monkewitz 1983; Cowley 1987; Monkewitz & Bunster 1987; Jensen, Sumer & Fredsoe 1989; Kurzweg, Lindgren & Lothrop 1989; Spalart & Baldwin 1989; Eckmann & Grotberg 1991; Fishler & Brodkey 1991). The reasons most frequently invoked for these studies range from search for physical insight as to how the transition process, bursting events, and turbulence production mechanisms are affected by flow periodicity to the potential application of the resulting understanding to the design of equipment and improvement of processes subjected to

transient or pulsatile flow conditions (e.g. heat and mass transfer over that in a corresponding steady flow, respiratory ventilators, turbomachinery and fluid control systems, wave-height damping and sediment movement by water waves, and transition to turbulence in the large arteries). The discussion of the relevant contributions will be taken up following the delineation of the fundamental parameters characterizing the flow.

1.2.1. *Governing parameters*

The oscillatory Reynolds number has taken many forms, but the most common one is $Re_\delta = U_{\max}\delta/\nu$, where $\delta = (2\nu/\omega)^{\frac{1}{2}}$ is proportional to the Stokes-layer thickness, $U_{\max}$ is the amplitude of the free-stream velocity ($u = U_{\max}\sin\omega t$), ν is the kinematic viscosity, and ω is the angular frequency of oscillation. Another relevant parameter when discussing oscillating flow in pipes is the Womersley number, $\alpha = R(\omega/\nu)^{\frac{1}{2}}$ or the Stokes parameter $\chi = R/\delta$ (R = radius of the pipe and $\alpha = \sqrt{2}\chi$) which expresses the importance of the radius of transverse curvature R relative to the boundary-layer thickness. These two parameters may be replaced by two other, more primitive, non-dimensional groups A/R (A = amplitude of the sinusoidal oscillation) and $R^2\omega/\nu$ as critical parameters in determining the structure of both laminar and turbulent oscillatory flows in tubes or over bluff bodies (Sarpkaya 1976, 1978).

Casarella & Laura (1969) and, subsequently, Chew & Liu (1988) compared the solutions of the Navier–Stokes equations for oscillatory flow along a circular cylinder and over a flat plate for various values of α and concluded that in the limiting case where $\alpha = \infty$, (i.e. for a cylinder of infinite effective radius), the solution for the cylinder case converges exactly, as expected, to that for the flat plate. A plot of the normalized radial-velocity amplitude versus $y(\omega/\nu)^{\frac{1}{2}}$ for various values of α shows that (Chew & Liu 1988) for $\alpha > 5$, the velocity amplitude is virtually the same as when $\alpha = \infty$. This observation is in full agreement with the experimental works of Hino *et al.* (1976) and Kurzweg *et al.* (1989). Casarella & Laura (1969) and Chew & Liu (1988) have also shown that the phase lead of the maximum wall shear stress over the maximum free-stream velocity for $\alpha = \infty$ converges to 45°, as in the case of a flat plate. For $\alpha = 5$, the phase lead is about 43°.

In the present investigation $\alpha = R(\omega/\nu)^{\frac{1}{2}} = 82$ (i.e. $\chi = R/\delta \approx 58$ with the cylinder radius $R = 76$ mm, $\omega = 1.174$ rad/s, and $\nu = 10^{-6}$ m^2/s). Thus, in the light of the foregoing, one can conclude that the stability of flow in the present investigation is governed by Re_δ only and the results should be comparable with those for flow over a smooth flat plate (e.g. Kamphuis 1975; Jensen *et al.* 1989; and the direct Navier–Stokes simulation of Spalart & Baldwin 1989) or flow within a pipe with $\alpha > 5$ (e.g. Hino *et al.* 1976). This does not, however, imply that the critical Reynolds number does not vary from experiment to experiment. Evidently, one cannot control or even recognize all possible secondary parameters which influence the state of the flow, particularly when the flow is on the verge of instability. Even under controlled laboratory conditions, the inception of low-speed streaks and hairpin vortices may be sensitive to and controlled by unknown and unknowable disturbances in the main flow which always exist in any experimental facility. As far as the inception of the first few streaks and hairpin vortices are concerned, the uplifting of the spanwise vorticity and its orientation relative to the streamwise direction may very well depend on the nature of the ambient flow, the type of disturbances it contains and the physical characteristics of the sublayer fluid.

1.2.2. *Comments on related stability studies*

Some of the earlier studies on oscillatory flows were concerned primarily with the definition of the boundaries between the laminar and turbulent flow regimes. For flow in pipes, Sergeev (1966), Merkli & Thomann (1975), Hino *et al.* (1976, 1983), Ohmi *et al.* (1982), Kurzweg *et al.* (1989), and Eckmann & Grotberg 1991, among others, have reported Re_δ^{crit} values (independent of χ) in the range of 500–550. Comparable values have been reported by Li (1954) ($Re_\delta^{\text{crit}} = 565$) and by Jensen *et al.* (1989) ($Re\ \text{crit}_\delta = 447$) for transition in Stokes flow over planar surfaces. However, Re_δ^{crit} values as low as 280 for flow in a pipe (Merkli & Thomann 1975) and 142 for flow over a plate (Kamphuis 1975) were also reported. These wide discrepancies between Re_δ^{crit} indicate that the instability is possibly subcritical, making transition strongly dependent upon the disturbance level in different facilities (Monkewitz & Bunster 1987).

More recent studies dealt with the nature and mechanism of the instability. Spalart & Baldwin (1989) carried out direct Navier–Stokes simulations of the oscillating turbulent boundary layer and found that the flow exhibits a first transition to a 'pre-turbulence' state just below $Re_\delta = 600$. A second transition, between 600 and 800, allows the flow to generate well-developed turbulence during at least part of the cycle. Fishler & Brodkey (1991) carried out a flow visualization study of the transitional and oscillatory flow in a rigid pipe through the use of tracer particles and high-speed motion pictures. Their Re_δ^{crit} was in the range 650–1000. The oscillatory transitional and turbulent flow structures were found to be very similar (but not necessarily identical) to the previously determined steady turbulent-flow structures (Corino & Brodkey 1969).

The theoretical studies yielded a variety of Re_δ^{crit} and the predictions ranged from full stability for all values of Re_δ to unconditional stability for only very low values of Re_δ. The quasi-steady theories (e.g. Collins 1963; Monkewitz 1983; Cowley 1987; Monkewitz & Bunster 1987) predict that the most dangerous profiles occur at the start of the acceleration phase whereas numerous experimental observations (e.g. Hino *et al.* 1976; Fishler & Brodkey 1991; Eckmann & Grotberg 1991) show that transition to turbulence occurs only in the decelerated part of the flow cycle, with violent bursts taking place towards the end of the deceleration phase (Hayashi & Ohashi 1982). The linear stability calculations by von Kerczek & Davis (1974) and by Hall (1978) predict that in the periodic steady state the oscillatory Stokes layer is absolutely stable to all infinitesimal disturbances.

There does not seem to be any theoretical or experimental study of the instability and transition of the external boundary layer (as opposed to usual pipe flow) along a cylinder immersed in a sinusoidally-oscillating flow. A comprehensive review of the turbulent boundary layer on a cylinder in axial flow is given by Lueptow (1990).

In the present work we wish to relate the inception of low-speed streaks and other turbulence structures to the Reynolds number through the use of flow visualization in an essentially unconfined flow. No flow statistics are offered, not because they are not important in identifying an instability mechanism, but because in the transition region 'the concept of turbulence as the random motions of small parcels of fluid would now seem quite untenable' (Head & Bandyopadhyay 1981) and the inception of the major constituents of wall turbulence deserve to be treated on their own merits.

2. Experimental apparatus and procedures

The primary goals for the equipment were to achieve a relatively large α in a sinusoidally-oscillating flow and to use non-intrusive means of measurement and flow visualization to quantify the inception and evolution of transition. The experiments were performed in a large U-shaped water tunnel. The working section is 145 cm high, 92 cm wide, and 10.7 m long. The two 6.7 m vertical sections are 183 cm × 92 cm each. A cross-flow microfiltration system was used to remove any suspended fine particles from the tunnel water (the filtration system was turned off during the experiments). The oscillatory flow in the tunnel is driven by an electronically controlled pneumatic system. The spectra of the velocity at various positions in the test section (obtained through the use of an LDV system) has shown that the contributions of the second and higher harmonics are indeed negligible. The transient period to reach a constant Re_δ from rest varies from 6 to 10 cycles for $Re_\delta < 2000$, with the fluid oscillating at its resonant period of $T = 5.3525$ s. Additional details of the design and operation of the tunnel are given elsewhere (Sarpkaya 1986*a*, *b*).

Normally, the amplitude of oscillations and hence the Reynolds number are transitioned from one value to another by enlarging or constricting an orifice in the pneumatic system. For the present experiments, however, a particular Reynolds number was set up in the tunnel either by gradually increasing the prevailing Reynolds number (set within the range 350–400 in order to start with a streak-free surface) or by starting the flow from rest (after a rest period of about an hour). The reasons for the two flow-establishment schemes were partly to explore the history effects on the evolution of coherent structures and partly to replenish the fluorescent dye which dissolves after many cycles of oscillation. Extensive observations and recordings with both schemes have shown that the streaks did not develop immediately after arriving at a new Reynolds number but took about 6 to 10 cycles to build up. The incipient structure and subsequent evolution of the resulting streaks were so similar that an independent observer could not have deducted from his observations and viewing of the video tapes as to how the new flow state was created, i.e. no history effects were observed.

The test cylinder (a long cigar-shaped body as shown in figure 1*a*) is 152 mm in diameter and 420 cm long (a central 210 cm long shear force sleeve, two 75 cm long dummy sections, and two 30 cm long sections of half bodies of revolution at the ends of the dummy sections for smooth geometrical transition). The entire test pipe is supported along its axis by a 10.7 m long stainless steel rod ($D = 25.4$ mm) running along the axis of the test section. An axisymmetric half-body analysis, based on a simple source and uniform flow representation, has shown that the velocity near the junction of the cylindrical section and one of the ends has returned to its ambient flow value for the geometry used. The length of the test cylinder was chosen such that it was at least six times the amplitude of flow oscillation; thereby ensuring that the flow about the shear force sleeve did not suffer from any end effects. This provision plus the shear stress and phase-angle data show, albeit indirectly, that neither the supporting rod nor the end sections had a measurable effect on the flow over the central test section.

A simple strain-gauge system, housed inside the test cylinder, was designed to record the shear force experienced by the force sleeve. The dummy sections were rigidly mounted to the support rod by a centring mechanism in order to align their axes exactly and overlap their edges with those of the test section. A gap of approximately 1 mm existed between the overlapping faces of the force sleeve and the dummy sections to allow freedom of movement of the force sleeve. The entire test pipe was designed to

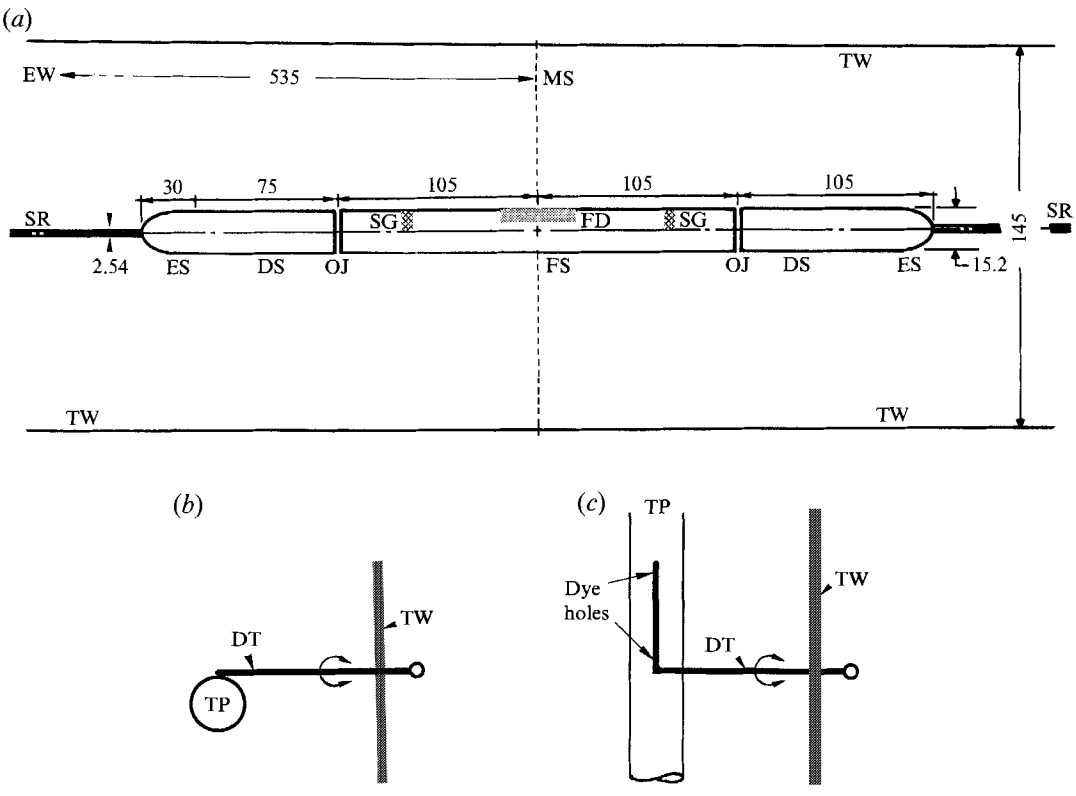

FIGURE 1. (*a*) Schematic side view of experimental set-up (dimensions are given in centimetres). DS, dummy section; ES, end section of test cylinder; EW, endwall of tunnel; FD, fluorescent dye; FS, force sleeve; MS, mid-section; OJ, overlapping joint; SG, strain gauges; SR, supporting rod; TW, tunnel wall. (*b*) Schematic cross-sectional view of dye introduction system. DT, dye tube; TP, test pipe; TW, tunnel wall. (*c*) Schematic plan view of dye tube and location of dye holes.

be neutrally buoyant in order to prevent the bowing of the support rod and misalignment of the dummy cylinder/force-sleeve interfaces. The heads of the countersunk screws were filled with wax, all components of the test pipe were carefully polished and painted black, and then polished again with pile velvet. Finally, the cylinder axis was initially aligned with the axis of the tunnel with an error less than 0.02° (i.e. with an error less than 2 mm from the tunnel axis between the two ends). At the completion of the experiments, the angle between the cylinder and the tunnel axis was gradually increased to about 4° in order to enhance the intensity of the perturbations in the ambient flow. These experiments have conclusively shown that neither the Reynolds-number range in which the streaks first occurred nor the character of the streaks have changed.

Calibration of the strain gauges was performed by two independent methods which yielded exactly the same value for a calibration constant. As the flow oscillated at a desired Reynolds number, the strain gauges yielded a time-dependent signal proportional to the sum of the shear force and the horizontal buoyant force (due to the pressure gradient) acting on the force sleeve. A differential-pressure transducer, connected to the pressure taps on the two legs of the tunnel (for details, see Sarpkaya 1976, 1986*a*), simultaneously indicated the acceleration experienced by the fluid. The small horizontal buoyant force is due to the differential pressure between the leading

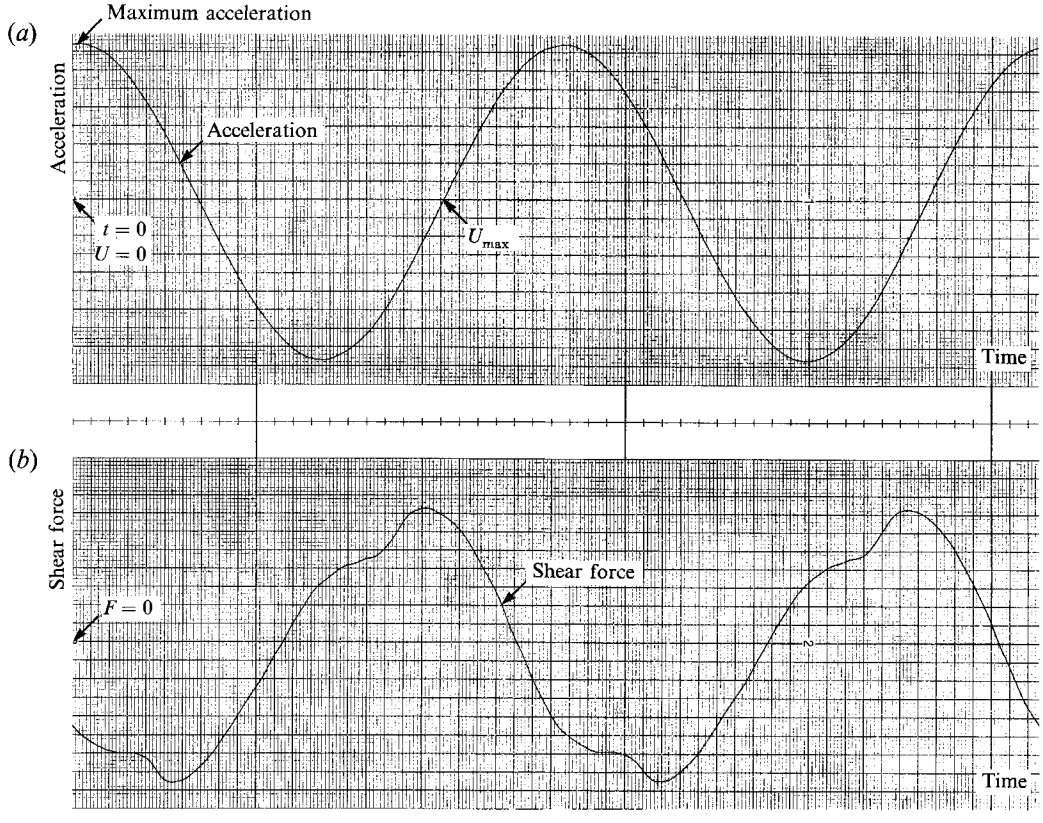

FIGURE 2. (*a*) Sample acceleration and (*b*) shear-force records ($t = 0$ at $U = 0$). $Re_\delta \approx 900$ and the phase lead of the maximum wall shear over the maximum free-stream velocity is about 13°.

and trailing edges of the 0.8 mm thick force sleeve. It is exactly proportional to the acceleration of the ambient flow and is electronically subtracted from the total force signal. The net shear force signal as well as the instantaneous acceleration were recorded, at least another 50 cycles beyond the transient period (6–10 cycles for $Re_\delta < 2000$), for 50 cycles at a sampling rate of 720 samples per cycle per channel (i.e. about 135 samples/second/channel or a sample for every 0.5°) through the use of a data-acquisition system. Figure 2 shows a representative shear-force trace together with the plot of the prevailing acceleration of the ambient flow for $Re_\delta = 905$ (the phase lead of the maximum wall shear over the maximum free-stream velocity is about 13°).

A portable laser sheet system, similar to that proposed by Koga, Abrahamson & Eaton (1987), has been set up to create a thin sheet of nearly collimated light which can be positioned at any angle desired relative to the cylinder or the ambient flow as shown in figure 3. The thickness of the light sheet was varied from about 1.5 mm to 5 mm (from about 30 wall units (ν/v^*, to be denoted by wu) to 100 wu in the range of Re_δ encountered). Here v^* is the wall shear velocity defined by $(\tau_w/\rho)^{\frac{1}{2}}$ (τ_w = wall shear stress and ρ = fluid density).

A grid was photographed in the plane of illumination at the start of each run in order to determine the relationship between the physical dimensions and the wall unit. The circumferential arc length (θ-direction) of the lighted area on the cylinder was varied from zero to about 1000 wu by moving the light sheet parallel to itself, i.e. toward and away from the tangent plane (figure 3*a*), through the use of a precision traversing

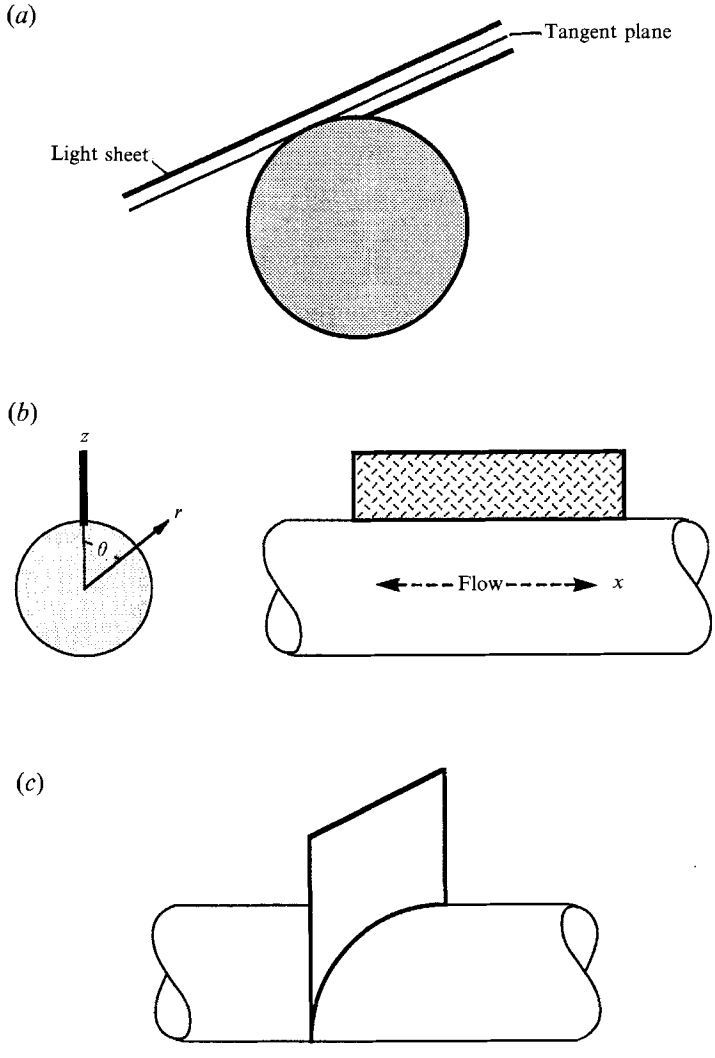

FIGURE 3. Sketch of the positions of the laser light sheet: (*a*) parallel to the tangent plane; (*b*) in the (z, x)-plane; and (*c*) intersecting the cylinder at a 45° angle.

mechanism. Normally, the lighted volume on the cylinder was about 40 wu thick, 700 wu wide (θ direction) and about 3000 wu long (x-direction). In a second series of experiments, the light sheet was placed in a vertical plane (z, x) to record the cross-section of the vortical structures in that plane (figure 3*b*). Finally, in another series of experiments, the light sheet was rotated about the z-axis to 'cut' the cylinder at a 45° angle (figure 3*c*). The length of the test section (10.7 m) made it nearly impossible to make a video recording of the flow structures in the transverse plane by placing the light sheet in the (z, r)-plane.

Fluorescent dye (mixture of water drawn out of the tunnel, unless noted otherwise, and a small amount of fluorescein powder, strained several times through a fine cloth) was introduced along a centrally-located 20–40 cm long section of the force sleeve with a retractable, L-shaped, remote arm (a 40 cm long, 3 mm diameter, closed-end tube, with uniformly spaced small holes along its length as shown in figures 1*b* and 1*c*). In a few cycles of oscillation, the dye distributed smoothly and uniformly over a known

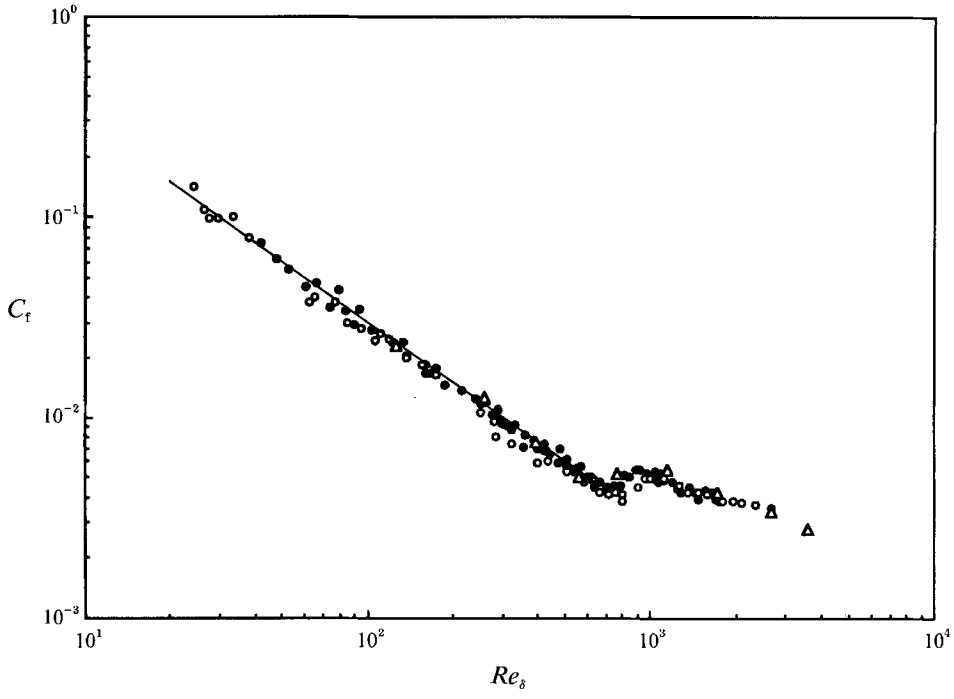

FIGURE 4. The amplitude of the normalized wall shear stress C_f *vs.* Re_δ: ——, Stokes theoretical prediction; ●, present data; ○, Kamphuis's data (1975); △, Jensen *et al.*'s data (1989).

area and remained there until upward fluid motions caused parts of it to lift. The evolution of the resulting low-speed streaks, hairpin vortices, and other flow structures were recorded on video tape simultaneously with the instantaneous acceleration of the ambient flow and time through the use of three video cameras and a screen splitter (two of the cameras operated at 60 f.p.s., and one at 500 f.p.s.).

At the completion of the shear force and flow-visualization experiments, a new, one-piece, neutrally buoyant, rigid test cylinder of identical shape and dimensions has been constructed (i.e. without the small gaps between the force sleeve and the dummy end sections), and the flow-visualization experiments have been repeated. The purpose of this time-consuming effort was to examine carefully whether the small gaps and the relative flexibility of the cylinder played any role in the creation and evolution of flow structures. The results have shown that the flow structures in the region of observation of the two test cylinders had no special distinguishing features attributable to the first or the second series of experiments. Subsequently, the one-piece cylinder was used to carry out flow-visualization experiments with dyes containing known amounts of glycerol (to increase shear) or methyl alcohol (to decrease shear), in addition to the tunnel water and fluorescein, for reasons which will be described later.

3. Discussion of results

3.1. *Shear stress and phase relationships*

The present experimental data for the amplitude of the normalized and time-averaged wall shear stress C_f versus Re_δ for an axially aligned cylinder are shown in figure 4 together with those obtained by Kamphuis (1975), using oscillatory waves over a smooth bed, and by Jensen *et al.* (1989), using a plate in a U-shaped water tunnel.

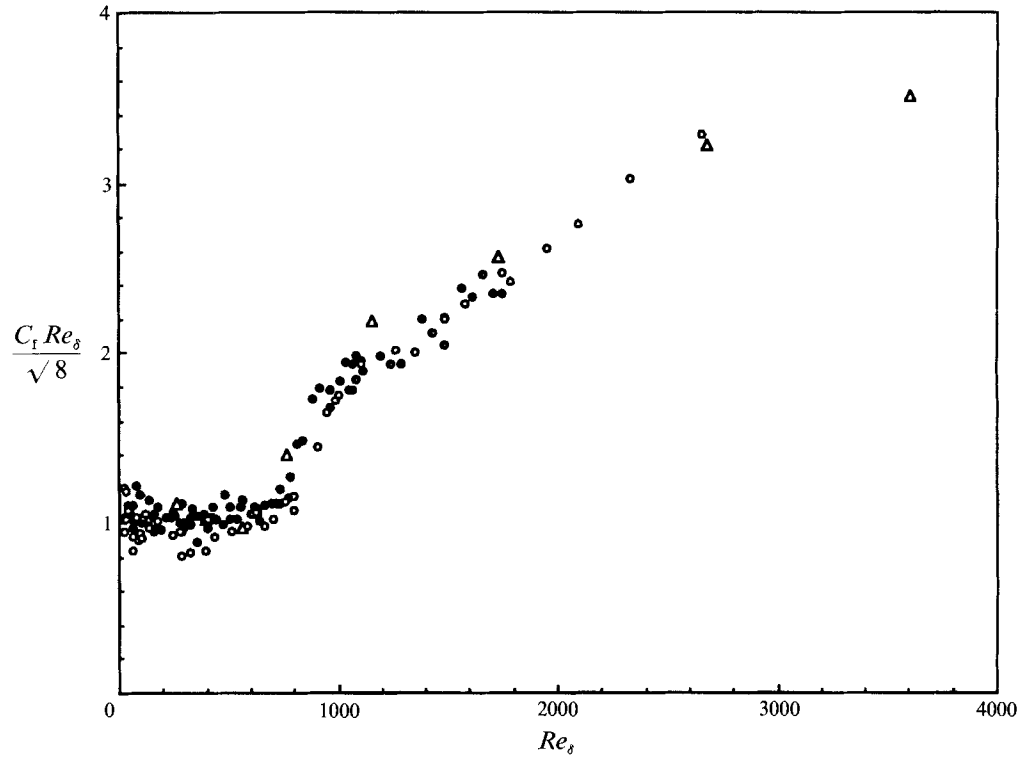

FIGURE 5. $C_f Re_\delta/\sqrt{8}$ as a function of Re_δ. Symbols are as in figure 4. Note that had the flow remained stable for all values of Re_δ, $C_f Re_\delta/\sqrt{8}$ would have remained constant at the theoretical value of 1.0.

These data are, with some minor exceptions, in good agreement with each other. The solid line where $C_f = \sqrt{8}/Re_\delta$ represent the Stokes value of C_f for laminar flow. It is noted that the theoretical and experimental results agree reasonably well for Re_δ smaller than about 400–600 (Kamphuis' data for $Re_\delta < 400$, present data for $Re_\delta < 500$, and Jensen *et al.*'s data for $Re_\delta < 570$).

Since C_f is given by $C_f = \sqrt{8}/Re_\delta$ in the laminar stable regime, it is more instructive to plot $C_f Re_\delta/\sqrt{8}$ as a function of Re_δ as shown in figure 5. Had the flow remained stable for all values of Re_δ, $C_f Re_\delta/\sqrt{8}$ would have remained constant at the theoretical value of 1.0. Even though it still is not clear from figures 4 and 5 where the instability first manifests itself, it is clear that C_f does not exhibit a measurable increase until Re_δ reaches a value of about 750–800. Only a mild increase in C_f is noticeable in Jensen *et al.*'s data at $Re_\delta \approx 800$. Kamphuis' data show a relatively sharper increase in C_f at $Re_\delta \approx 800$.

The relation of the rapid variation in C_f to the phase angle sheds further light on the transition process. Figure 6 shows the phase lead of the maximum shear stress over U_{max}. Also shown in figure 6 are the data of Jensen *et al.* (1989), Hino *et al.* (1983), and Spalart & Baldwin (1989) (from a direct Navier–Stokes simulation). Clearly, the phase angle begins with its theoretical value of 45°, as expected, and remains nearly constant up to $Re_\delta \approx 400$. Then it decreases gradually to about 33° at $Re_\delta = 750 \sim 800$. This coincides with the start of a measurable increase in C_f. In the range of Re_δ, say from about 780 to 880, the phase lead sharply drops to about 13°.

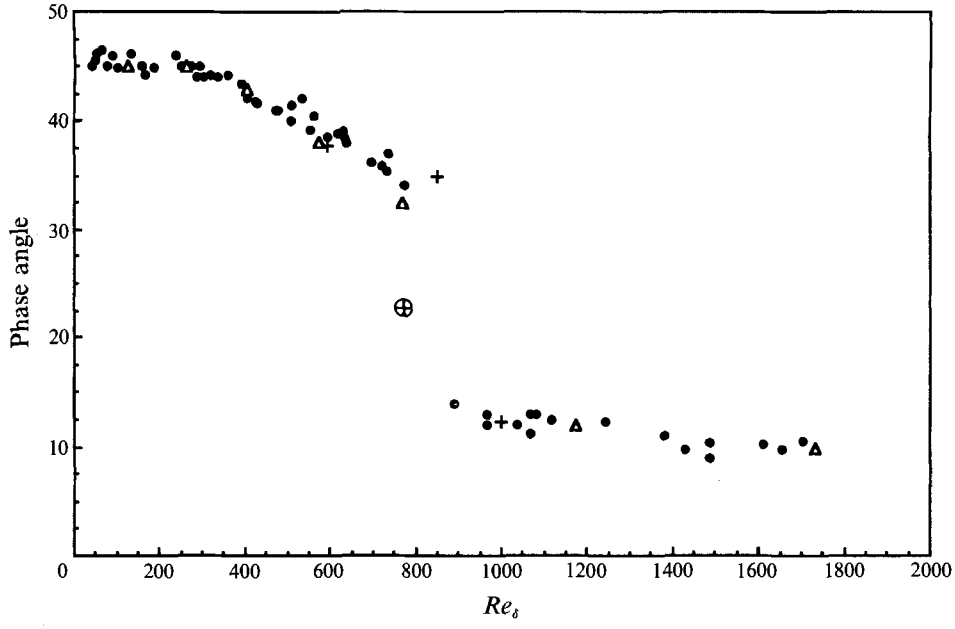

FIGURE 6. The phase lead of the maximum shear stress over the maximum velocity: ●, present data; △, Jensen *et al.*'s data (1989); ⊕, Hino *et al.*'s data (1983); +, Spalart & Baldwin's direct Navier–Stokes simulation (1989). Note that the phase angle begins with its theoretical value of 45° and remains nearly constant up to $Re_\delta \approx 400$. Then it decreases gradually to about 33° at $Re_\delta = 750 \sim 800$. This coincides with the start of a measurable increase in C_r, shown in figure 4. In the range of Re_δ, from about 780 to 880, the phase lead sharply drops to about 13°.

3.2. *Evolution of quasi-coherent structures*

The description to follow is based on extensive video viewing and the information extracted from it in terms of occurrence of various types of structures, mindful of the fact that the vagaries of flow visualization do not always provide correct insight into the physics of the actual occurrences. Furthermore, one can only repeat the complaint registered by practically all experimenters on this subject that still photographs (taken directly from the video screen using conventional photography or a videographic copier) do not convey as much information as motion pictures.

When the flow was set at $Re_\delta \approx 400$ (either by gradually increasing the Reynolds number, from about 350, or by starting the flow from rest), one or more unevenly spaced low-speed streaks emerged (at new transverse positions) toward the end of each deceleration period. They remained perfectly straight, smooth, and parallel (to each other and to the ambient flow), moved small amounts toward and away from each other with no visible interaction, and then completely disappeared during the acceleration period, i.e. the dye surface became mirror smooth in the later stages of the acceleration period and remained so in the earlier stages of the deceleration period. This repetitious process was visible as long as the dye lasted (for at least sixty cycles of flow oscillation) with no hairpins, no arches, no interaction between the streaks, and no conspicuous indications of vortical structures of any form or shape in any of the three planes of observation (see figure 3). In other words, no quasi-coherent structures have emerged from the sublayer. This simple experiment was repeated at the start of each test day, at least three hundred times during the past four years.

When the Reynolds number was set in the range $Re_\delta \approx 420$–460, a most interesting series of events was observed in one or more low-speed streaks toward the end of the

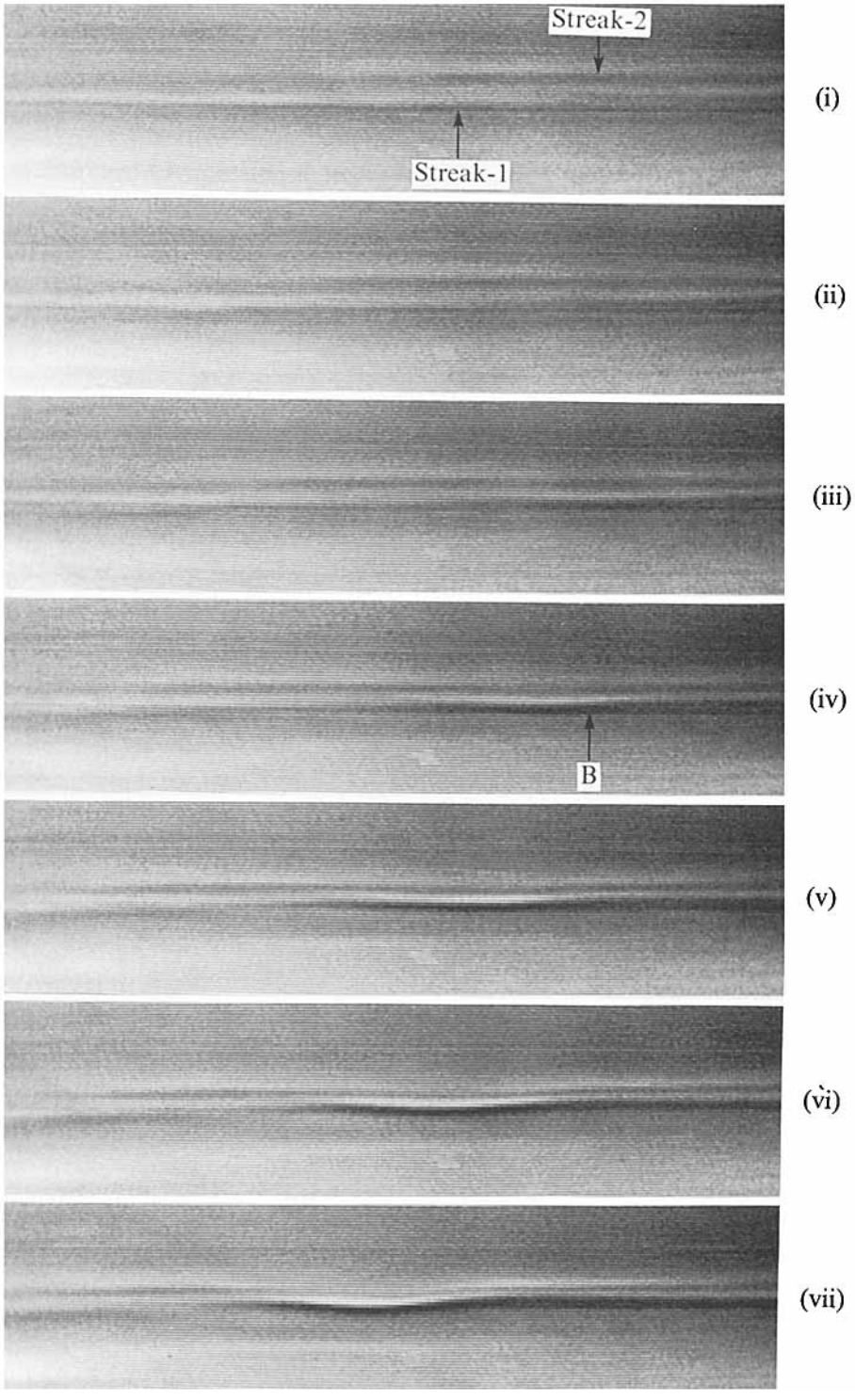

FIGURE 7(i–vii). For caption see p. 121.

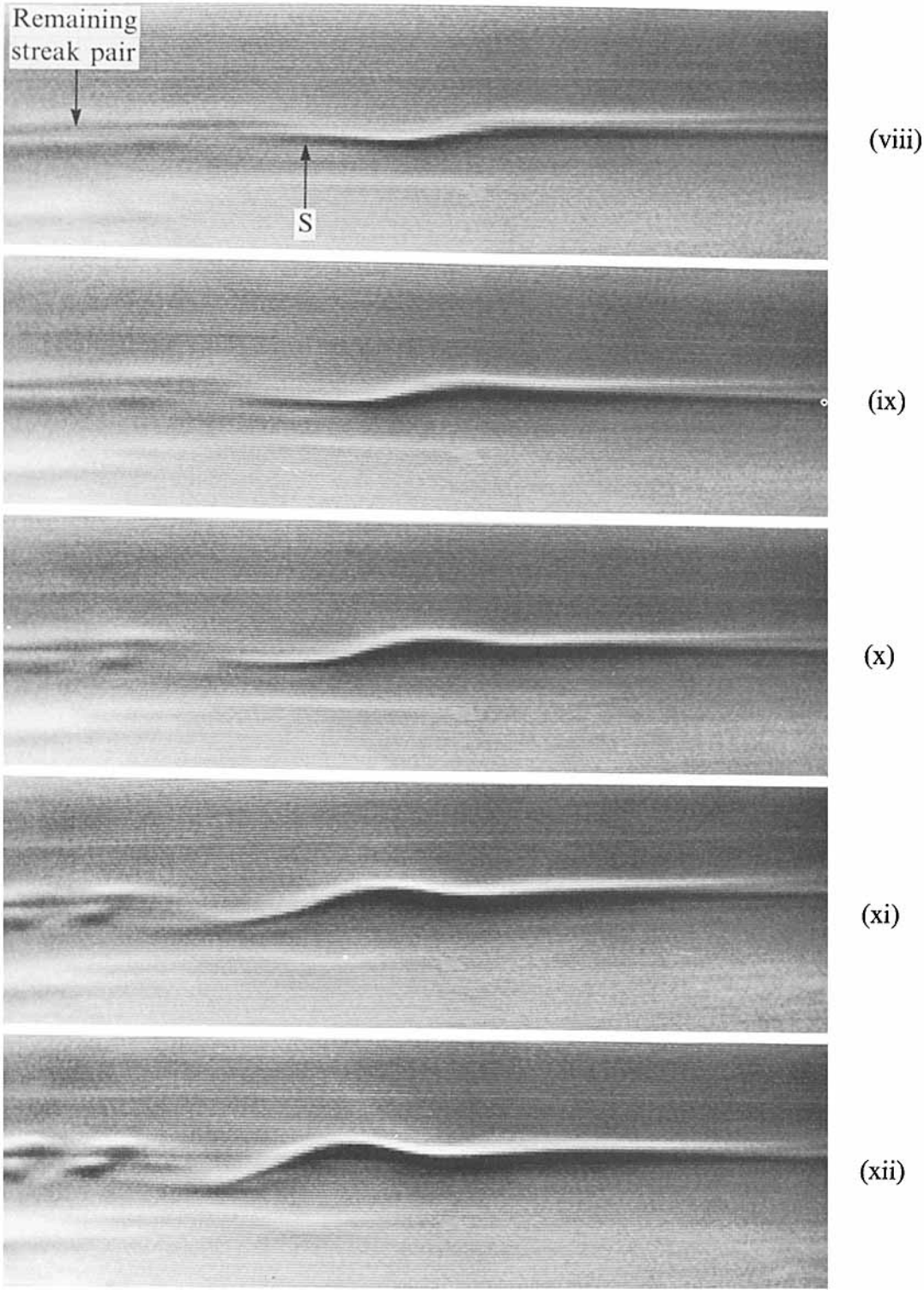

FIGURE 7(viii–xii). For caption see p. 121.

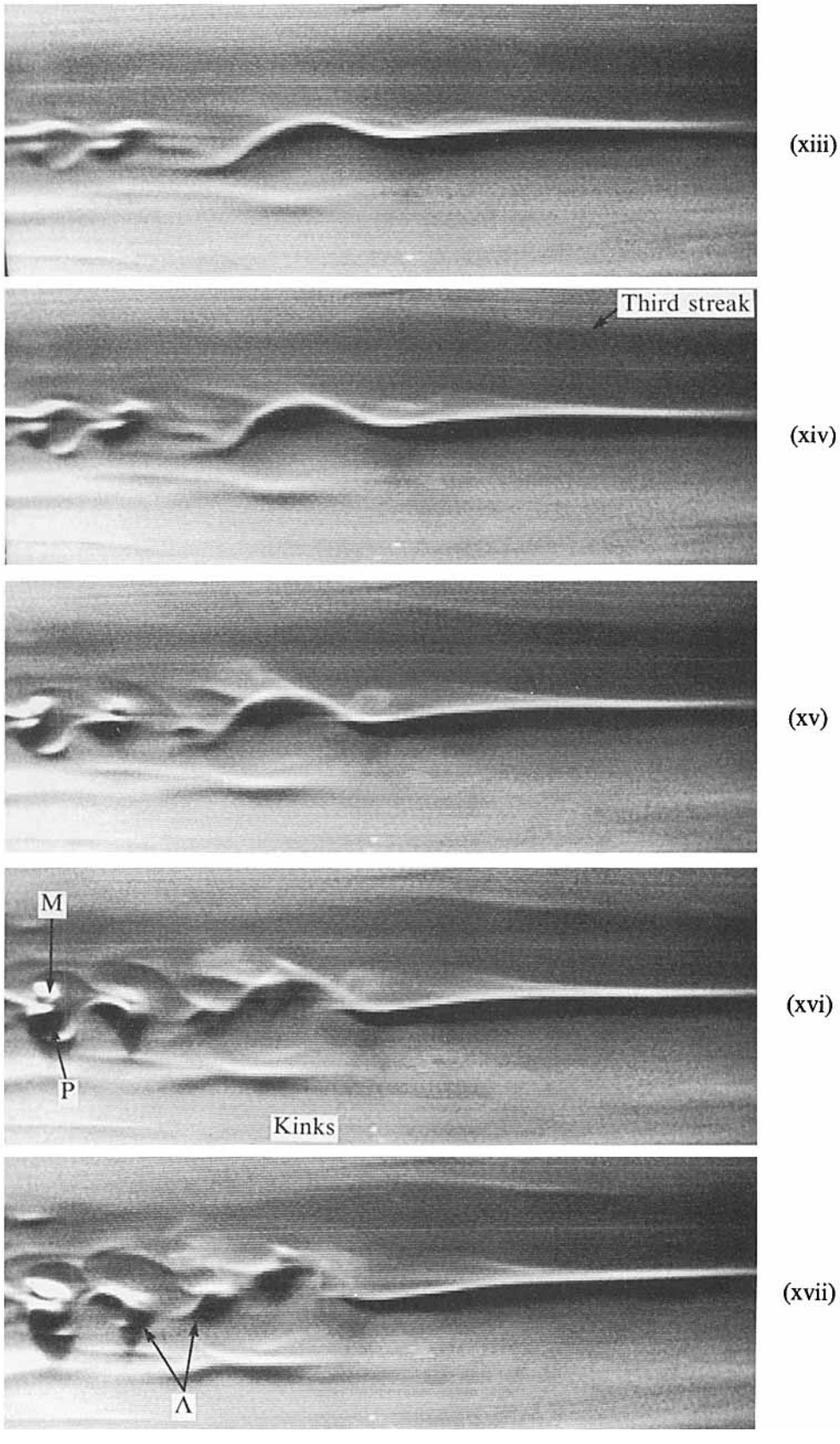

FIGURE 7(xiii–xvii). For caption see p. 121.

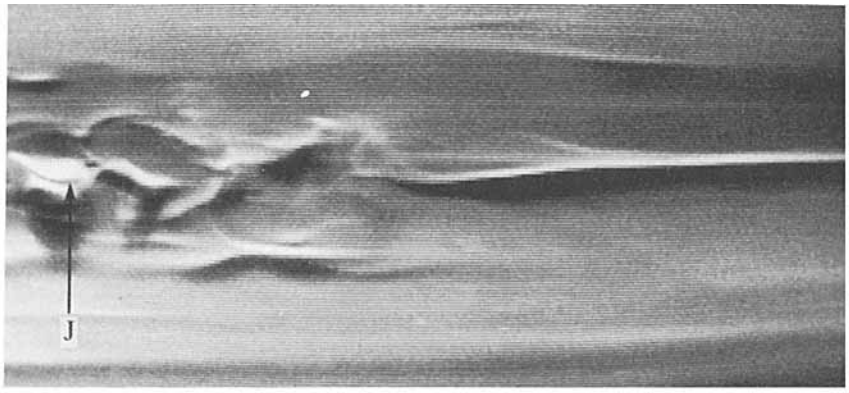

(xviii)

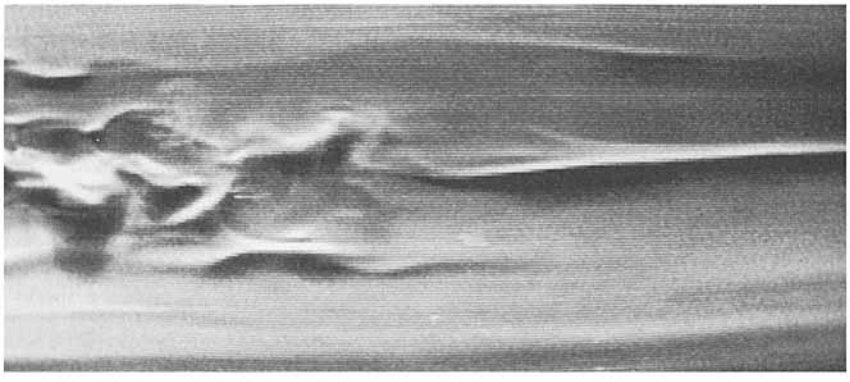

(xix)

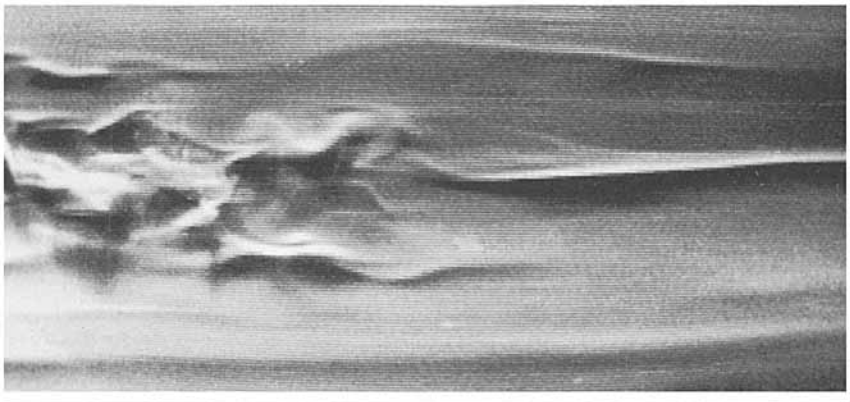

(xx)

(xxi)

FIGURE 7(xviii–xxi). For caption see p. 121.

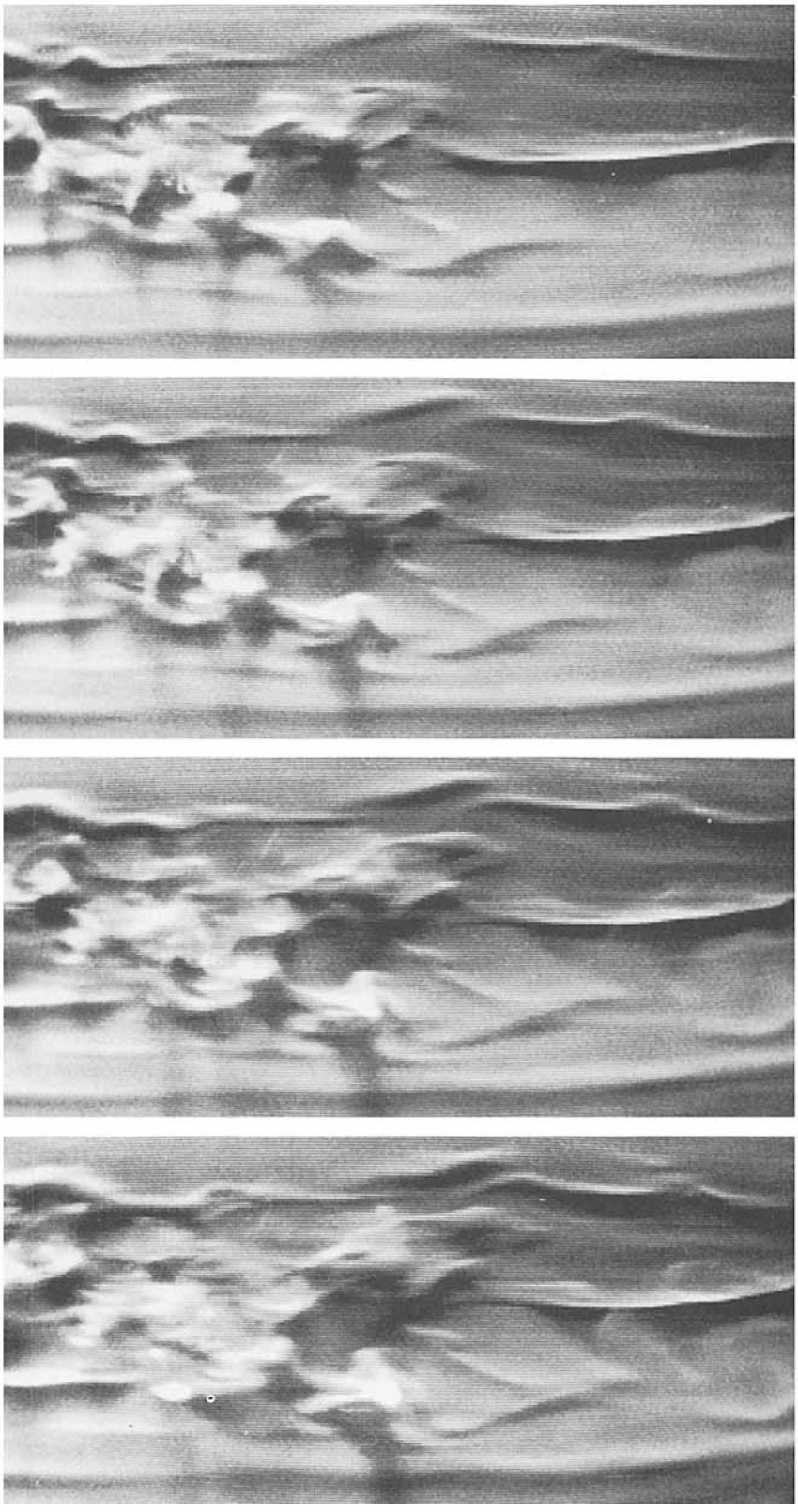

FIGURE 7(xxii–xxv). For caption see facing page.

deceleration period, at about $t^+ (= tv^{*2}/\nu) \approx -150$ to -175. Here the time is measured from the point $U = 0$, i.e. from the beginning of the maximum acceleration (see figure 2), and the time unit is defined as $\text{tu} = \nu/v^{*2}$ (one quarter of the flow oscillation period is about 500 tu for $Re_\delta = 440$).† It must be emphasized that the first streak 'seen' in the area of observation is not necessarily the first streak occurring anywhere on the cylinder. The observations and times recorded below concern the evolution of structures occurring only in the volume of observation (approximately 40 wu in the r-direction, 700 wu in the θ-direction, and 3000 wu in the x-direction).

For the particular realization described below, a single streak came into existence at about $t^+ \approx -262$. At $t^+ \approx -250$ another streak (identifiable by the naked eye) was born at a distance of about 120 wu. They have moved, slowly at first and rapidly thereafter, toward each other (the lower one upward and the upper one downward in the (x, θ)-plane). Meanwhile, both streaks grew in amplitude and remained parallel throughout their observable length. At time $t^+ \approx -175$, they have reached the size and positions shown in figure 7(i) (succeeding frames are 12.5 tu apart). The frames between $t^+ = -250$ and $t^+ = -175$ are not shown here simply to conserve space. With the exception of their spacing, the streaks were nearly identical to those shown in figure 7(i). At $t^+ = -150$, a small bulge appeared in the lower streak (labelled B in figure 7iv, it is barely visible in figure 7iii) where the two streaks began to coalesce. (The streak merging or coalescence was also seen in Rashidi & Banerjee's (1990) experiments and considered to be quite important for $10 < y^+ < 30$.) At $t^+ \approx -100$ (figure 7viii), the merging of the streaks upstream of S is almost complete (except at the far right of S). The amplitude and curvature of the combined streak (or the sinuous streak) increased rapidly, as evident by the intensification of the contrast between the bright and dark regions. In the meantime, a gap developed between the downstream end of the sinuous streak and the remainder of the original streak pair (to the left of S), as seen clearly in figure 7(viii) at $t^+ \approx -88$. The end of the sinuous streak terminated between the two outboard-flanking remainders of the first and second streak. Shortly thereafter, the remaining streak pair began to split into shorter segments (see e.g. figures 7ix–7xii). These, in turn, acquired larger amplitudes (labelled M in figure 7xvi) in the decelerating flow, drained the dyed fluid in their vicinity, and gave rise to nearly symmetrical 'pockets' (Falco 1991) or heart-shaped darker regions (labelled P in figure 7xvi). Note that the structures labelled M (originating from the ridges of two separate streaks) are not hairpin vortices. Their tips did not seem to be joined until the coherent structures became more chaotic (labelled J in figure 7xviii).

The sinuous streak has undergone rapid changes also. What is not immediately visible (at least in a still frame) is that the crest of the sinuous streak began to 'break'

FIGURE 7. Time sequence of the evolution of two parallel streaks into a sinuous streak plus other structures in the area of observation of the video camera (fixed in laboratory coordinates). The flow is from right to left. Figure 7(i) is at $t^+ \approx -175$ and figure 7(xxv) is at $t^+ = +125$, (frames are 12.5 time units apart). The plane tangent to the cylinder bisected the light sheet, as shown in figure 3(*a*). B (in 7iv) is the position of the initial bulge, S (in 7viii) denotes the end of the sinuous streak, M (in 7xxvi) is the position of the growing remnants of the original streaks, P (in 7(xxvi)) is the location of one of the 'pockets', Λ (in 7xvii) shows the evolution of Λ-shaped structures, and J (in 7xviii) shows the apparent joining of the tips of two structures.

† The flow ($U = U_{\max} \sin \omega t$) moves from left to right in the interval $0 < \text{tu} < 1000$ and from right to left in the interval $1000 < \text{tu} < 2000$, for $Re_\delta = 440$. The acceleration and deceleration phases alternate every 500 tu: Acceleration ($0 < \text{tu} < 500$); deceleration ($500 < \text{tu} < 1000$); and then, in the reverse direction, acceleration ($1000 < \text{tu} < 1500$); and deceleration ($1500 < \text{tu} < 2000$). Thus, -150 tu and 1850 tu are identical instants, separated by one cycle.

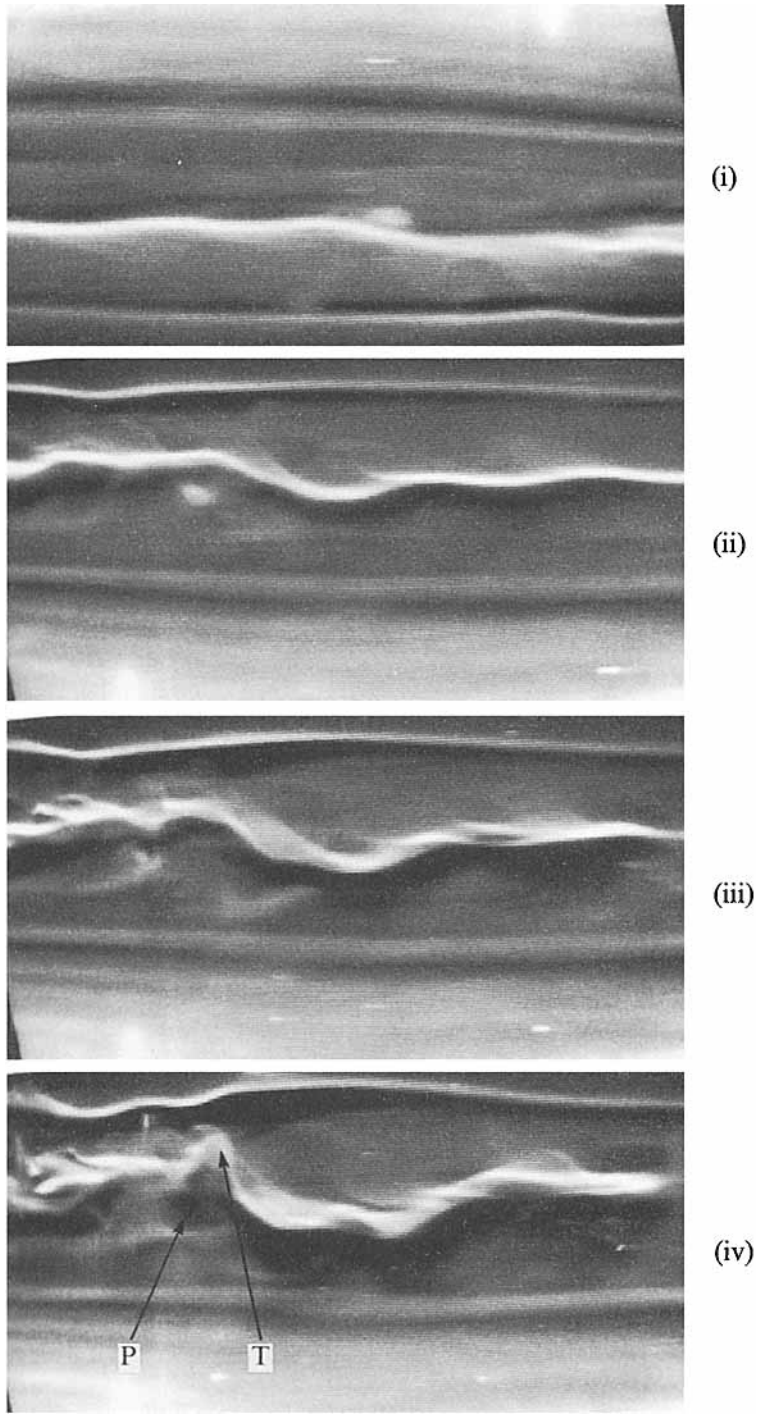

FIGURE 8(i–iv). For caption see facing page.

and the decelerating streamwise flow began to lift over the inclined portions of the streak which decelerated even faster than the ambient flow. This led to the formation of quasi-streamwise vortices on the downstream side (lighter side) of the streak. This action is clearly visible in figures 7(xiv) and 7(xv) (where the ambient flow experienced

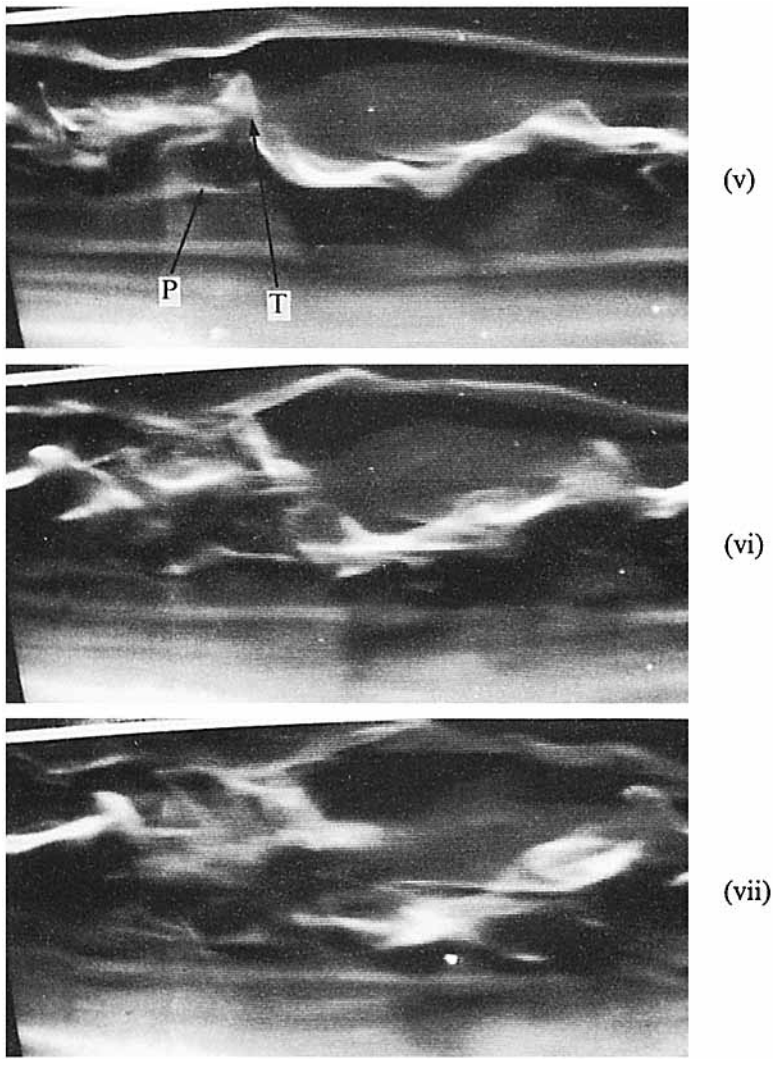

FIGURE 8. The evolution of three low-speed streaks (135 to 160 wall units apart) in the region where the sinuous streak and the rest of structures (figure 7) occurred in the previous cycle (the flow is again from right to left). P and T (in 8iv and 8v) denote, respectively, the 'pockets' and 'tongues' (Λ-shaped structures).

maximum deceleration). Figures 7(xv)–7(xvii) show the development of kinks and the formation of Λ-shaped structures or vortex sheets (labelled Λ in figure 7xvii). The Λ-shaped structures have been frequently called Λ-vortices (see e.g. Yang, Spalart & Ferziger 1992). Our observations lead us to suggest that they are Λ-shaped vortex sheets which could roll-up into Ω-shaped hairpin or horseshoe vortices if the prevailing conditions (sufficiently high unidirectional shear and time) are conducive to such a development (see also Perry, Lim & Teh (1981) for Λ-shaped structures and Sarpkaya (1983) for horseshoe vortices). The line connecting the tips of these structures in figures 7(xvi)–7(xviii) makes an angle of $\lambda = 22°$ with the flow direction (fifty randomly selected realizations yielded $\lambda = 20° \pm 3°$).

The Λ-structures surged upward and forward (to the right in figures 7xvi and 7xvii) for about 20 tu to 30 tu, at a speed faster than the ambient flow, in the early

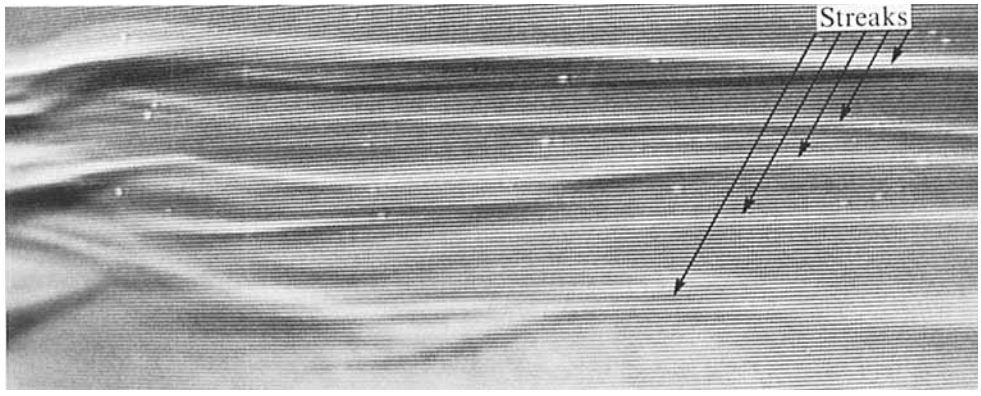

FIGURE 9. An example of the multiple-streak formation when the flow is allowed to continue to oscillate. These streaks (at least five, some are lifting) are not a multiplication of the previous streaks. They are born almost simultaneously, shortly before the time of maximum deceleration, in an otherwise smooth region of the dye-covered area (flow is from right to left). Their spacing ranges from about 85 to 135 wall units.

stages of the acceleration phase.† Thus, for a brief moment the ambient flow appeared to be decelerating relative to the structures, even though it was accelerating in the same direction. Subsequently, as the velocity of the ambient flow increased, the lifted portions of the Λ-structures folded back, stretched rapidly, and became incoherent structures (figures 7xviii and 7xxi). The duration of their destruction was about one fourth the time of their development. It seems that several factors such as the inception of the sinuous instability during a relatively brief period toward the end of the deceleration phase, unavailability of sufficient time for the Λ-shaped sheets to roll-up into Ω-shaped vortices, and the reversal of flow, which precipitates the destruction of coherent structures, are primarily responsible for the occurrence of fewer *hairpin* vortices in oscillating flows relative to those in canonical flows. (This conclusion is based on a conservative comparison of the independent viewing of our low-speed (60 f.p.s.) and high-speed (500 f.p.s.) video tapes (by three observers over a period of four years) with the information gleaned from the ciné films and detailed descriptions of Head & Bandyopadhyay (1981). Recently, Sandham & Kleiser (1992, p. 345) concluded that 'hairpin vortices are the exception, rather than the rule, for the vortices that develop from the high-shear layer around each Λ-vortex. The simplified statement, often found in the literature, that the high-shear layer rolls up into hairpin vortices, is therefore a little misleading.')

Figure 7(xiv) and those that follow show the inception of another streak (on the brighter side of the first streak, at a distance of about 140 wu). The events following the inception of a sinuous streak are, indeed, very similar to those described by Jimenez & Moin (1991) in connection with the evolution of their 'minimal flow unit', in their direct numerical simulation of unsteady channel flow (see their figures 25 and 26).

As the flow began to accelerate from left to right and approached the 25% mark of its acceleration period ($t^+ = 125$, figure 7xxv), most of the identifiable features of the structures became smeared (partly due to their faster convection in front of a fixed camera and partly, and more importantly, due to their actual decay, as seen in video images taken at 500 f.p.s.) and a number of relatively short low-speed streaks at various angles relative to the ambient velocity have emerged. As the flow accelerated

† The phase lag ϕ for a fluid oscillating sinusoidally over a stationary wall is: $\phi = \sin^{-1}\{[e^{-y/\delta}\sin(y/\delta)]/[1-e^{-y/\delta}\cos(y/\delta)]\}$ (see e.g. Panton 1984, p. 270).

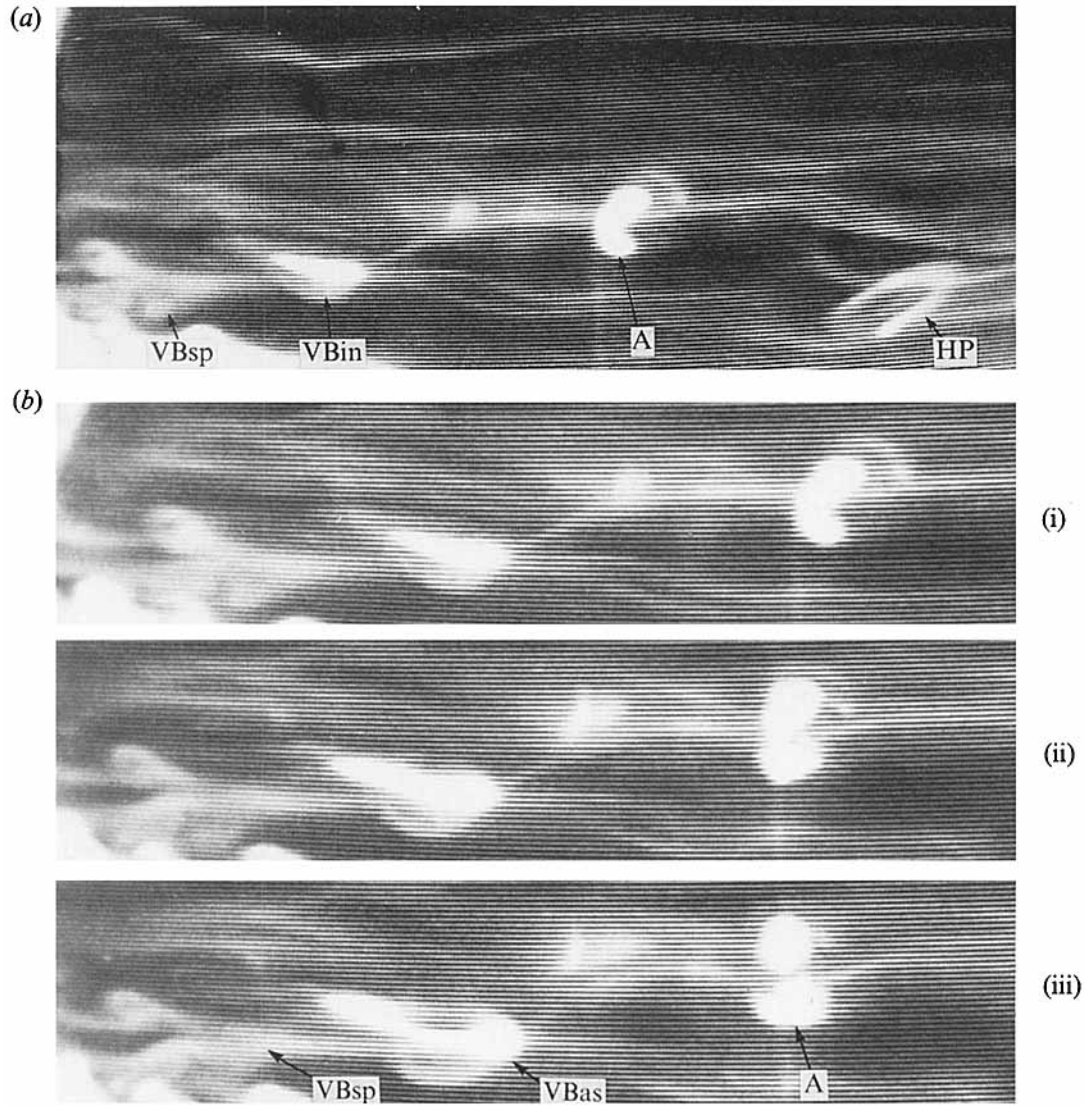

FIGURE 10. (*a*) A close-up view of an arch (A), a hairpin (HP), and a rarely-observed vortex breakdown: VBin shows the inception of the non-axisymmetric vortex breakdown and VBsp shows the spiral tail of the breakdown and its breakup into incoherent structures. (*b*) The evolution of the vortex breakdown over a short time period (successive frames are 12.5 time units, tu, apart). (i) corresponds to that shown in figure 10(*a*). Note that the nearly-axisymmetric breakdown (VBas) is followed by the usual spiral breakdown (VBsp).

further, the structures began to disappear quickly. In fact, at 250 tu the remaining few white patches (which resembled blossoming white chrysanthemums) simply convected across the observation site with no visible deformation. Finally, near 500 tu (end of the acceleration period), the dye sheet nearly returned to its original smooth state and remained so until about 700 tu (or -300 tu from the moment of the next maximum deceleration).

The type of streak evolution described in conjunction with figures 7(i)–7(xxv) repeated itself often enough but not always the same way, even when each experiment was started anew after a sufficiently long waiting period (say about an hour). From

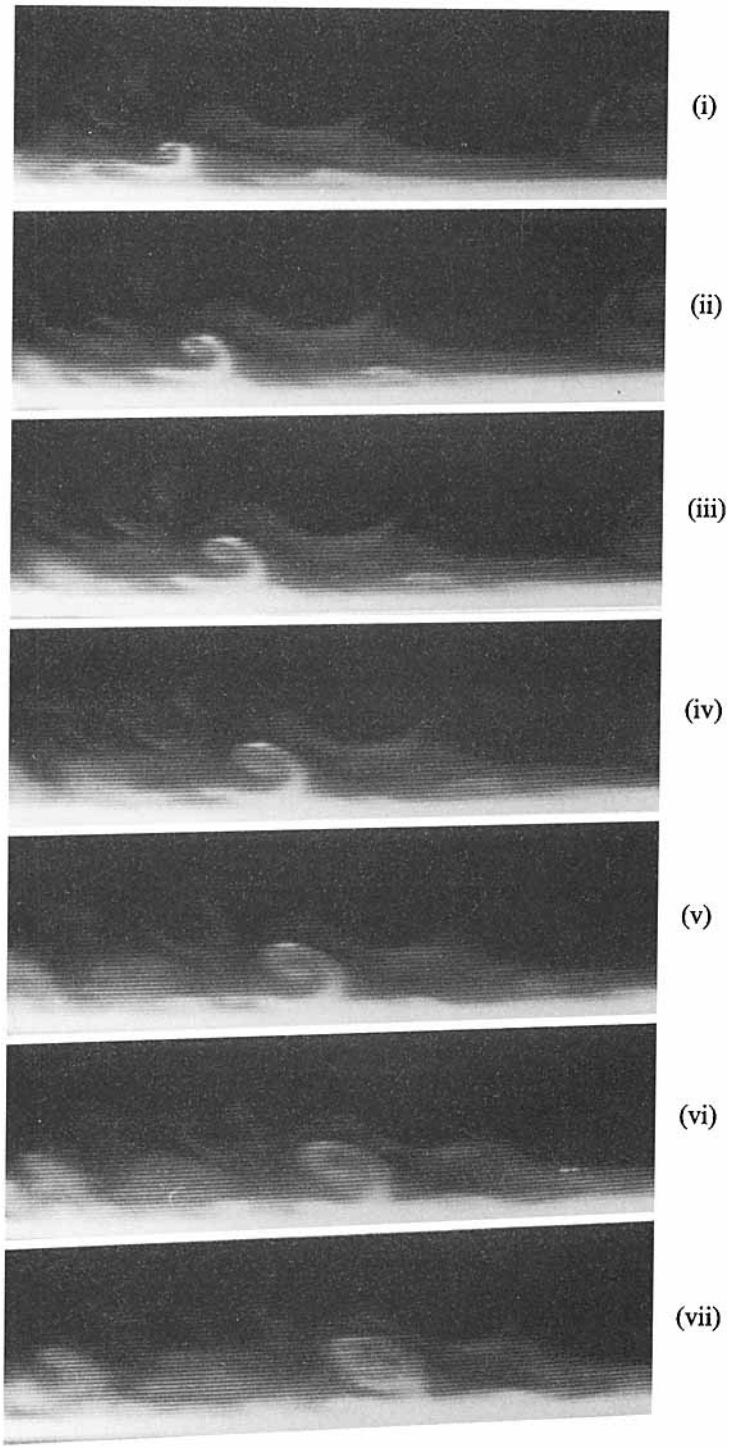

FIGURE 11. A close-up view of the evolution of one of the vortices, shortly after the flow began to accelerate to the right ($Re_\delta \approx 460$, the frames are about 13 time units apart.) The vortex had been created towards the end of the deceleration period (at about -130 time units) during which the structures near the wall were decelerating faster than the ambient flow. The vortex in (i) (at $+65$ tu)

time to time (for about 10% of the streak experiments in the range $Re_\delta \approx 420$–460), a single smooth streak, aligned approximately in the streamwise direction, came into existence, developed three-dimensional sinusoidal waves (often three or four nearly stationary waves in the volume of observation), and then evolved as described earlier (formation of quasi-streamwise vortices on the downstream side of the inclined parts of the streak, upstream travelling kinks, and the formation of Λ-shaped structures, eventually leading to incoherent structures).

If an experiment were continued at the same Re_δ, beyond the cycle at which a sinuous streak evolved, (say, to times beyond about 750 tu or 1750 tu), never again did a similar streak emerge, at least not in the volume of observation. Instead, two or more streaks came into existence almost simultaneously. These were the same type of streaks that occurred from time to time even when the experiment was started anew and the streaks in the area of observation were the first ones to emerge. These streaks did not coalesce but experienced considerable mutual interaction when they began to develop their own kinks, Λ-shaped structures, and pockets. It is possible that the streaks born in nearby regions (unseen by the camera) can sufficiently contaminate the flow so as to affect the type and nature of the observed streaks.

Figures 8(i)–8(vii) show the evolution of three streaks (135 wu to 160 wu apart) in the region where the single sinuous streak (figure 7viii and the rest) occurred in the previous cycle (the flow is again from right to left). Figure 8(i) (at 888 tu or at −72 tu from the moment of the next maximum deceleration) shows that the middle streak already began to 'break' or spill over (as in figures 7xv–7xvii) and develop three-dimensional oscillations (clearly visible in video). Figure 8(iv) (at −24 tu) shows the intensification of the turning, twisting, and toppling of the middle streak and the breaking of the upper streak. The lifting of the streak in the form of a 'tongue' or Λ-shaped structure (labelled T in figures 8iv and 8v) and the development of dark pockets are clearly visible. As the flow approached maximum deceleration (figure 8vi at −12.5 tu and figure 8vii at 0.0 tu), the top and middle streaks blossomed into complex shapes. The third streak never grew large enough to undergo breaking and disappeared soon after the flow began to accelerate.

Figure 9 is another example of the multiple-streak formation in subsequent cycles when the flow is allowed to continue to oscillate. The fact should be emphasized that these streaks (at least five) are not a multiplication of the streaks seen in previous cycles. They are born almost simultaneously, shortly before the time of maximum deceleration, in an otherwise smooth region of the dyed area (flow is from right to left). Their spacing ranges from about 85 wu to 135 wu. Figure 9 is not as sharp and detailed as figures 7 or 8 simply because the fluorescent dye began to dissolve. Nevertheless, one can see (as much as possible in a still photograph) that the downstream ends of the streaks began to lift off. In subsequent frames, the streaks went through motions very similar to those described previously (merging, tongues, pockets, occasional hairpins, oscillations, breaking, etc.). Figure 10(*a*), a close-up view of one of the subsequent frames, shows an arch over one of the streaks (labelled A), a hairpin on another streak (labelled HP), and a rarely observed vortex breakdown (labelled VBin, for the inception of the breakdown, and VBsp, for the spiral tail) above a region where the streaks appear to be merging. The fact that it is a vortex breakdown can only be proved by playing the video tape. Nevertheless, figure 10(*b*) is offered to show the evolution of the vortex breakdown over a short time by combining three successive frames

surge forward (and upward), for about 40 tu, at a speed faster than the ambient flow. Subsequently, the vortices and the ambient flow begin to move at about the same velocity and the vortices begin to flatten and become less cohesive as seen in (vii) (at 143 tu).

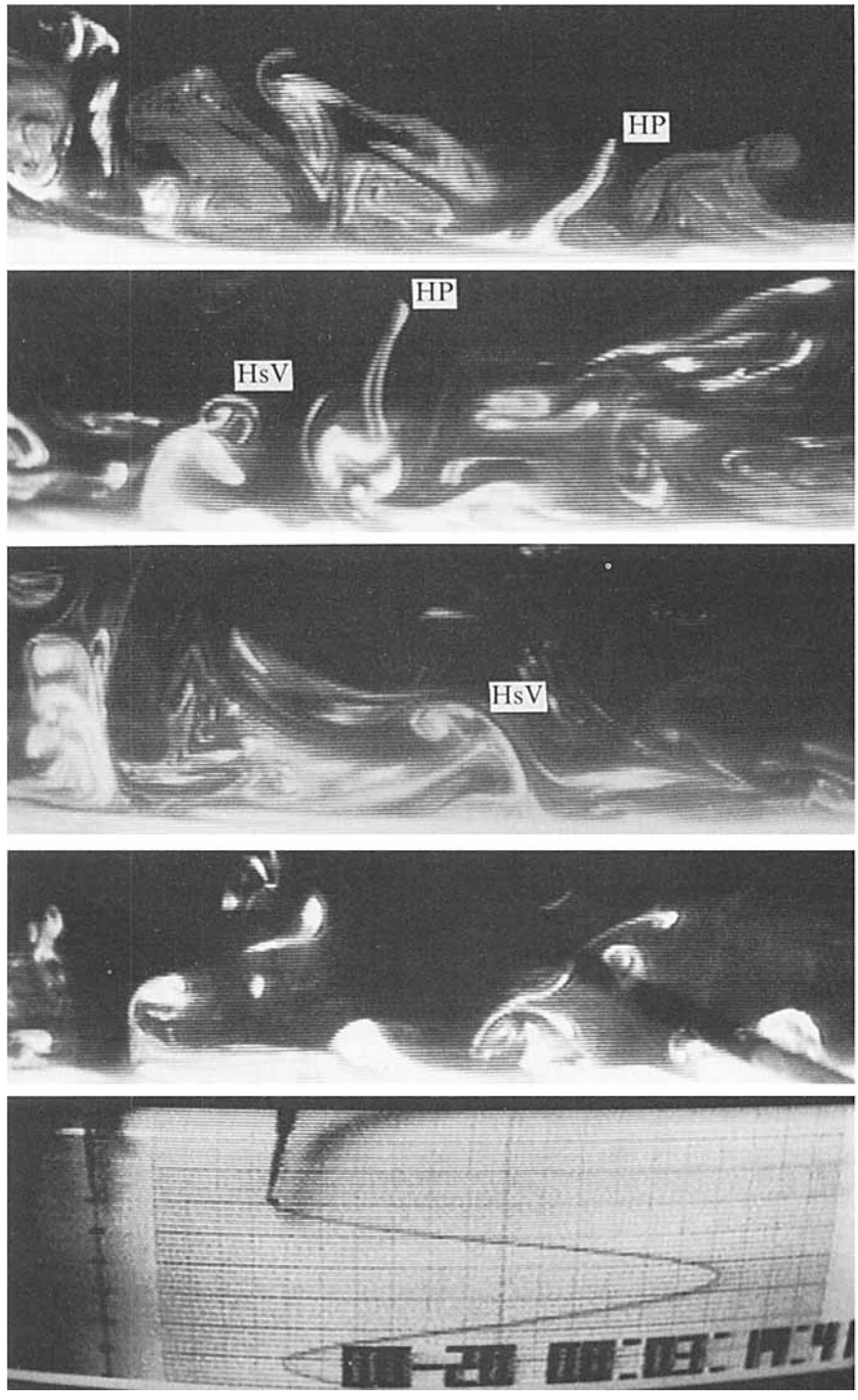

FIGURE 12. Sample close-up photographs of the vortical structures in the (z, x)-plane (Re_δ ranged from 490 to 520). Only two hairpin vortices may be seen in these figures (marked HP in (i) and (ii)). HsV (in (ii) and (iii)) shows sample heterostrophic vortices. (v) shows sample acceleration trace and digital time.

(12.5 tu apart) ((i) corresponds to that shown in figure 10*a*). The nearly-axisymmetric breakdown (labelled VBas in figure 10(*b*)(iii)) is followed by the usual spiral breakdown, clearly visible in all three frames (see Sarpkaya 1971).

When Re_δ was increased to about 460–490, a large number of vortices (not necessarily transverse) appeared in the (z, x)-plane. Figures 11(i)–11(vii) (about 13 tu apart) show a close-up view of the evolution of one of these vortices, shortly after the flow began to accelerate to the right. The vortex had been created towards the end of the deceleration period (at about -130 tu) during which the structures near the wall were decelerating faster than the ambient flow. A similar observation was previously made by Fishler & Brodkey (1991). The information deduced from the video pictures has shown that the vortex in figure 11(i) (at $+65$ tu) surges forward (and upward), for about 40 tu, at a speed faster than the ambient flow. In fact, the analysis of the motion of other structures, which have burst into existence at the later stages of the deceleration phase, has shown that they too surge forward relative to the ambient flow, at the early stages of the acceleration phase. Subsequently, the vortices and the ambient flow begin to move at about the same velocity and the vortices begin to flatten and become less cohesive as seen in figure 11(vii) (at 143 tu). As the velocity of the ambient flow increases further, the vortical structures begin to move with an average velocity slightly smaller than that of the ambient flow. The turbulent structures do not always survive the relaminarization efforts of the acceleration. The question of whether there will be residual or fossil turbulence during part of the acceleration period is dictated, at least in the present case, by Re_δ. As noted by Ramaprian (1984), 'The stabilizing and destabilizing effects during the two halves of the oscillation cycle may not (and do not in general) exactly cancel each other and thus there will be, in general, a net effect of imposed unsteadiness on the process of transition.' In other words, the flow can be successively laminar, transitionally-turbulent and laminar again.

When Re_δ was increased further to about 490–520, the rolled-up vortices became even more numerous over larger portions of the deceleration period and penetrated further into the ambient flow (figures 12i–12iv). The last frame shows the acceleration trace and time for figure 12(iv). These figures are chosen randomly from different runs in the Reynolds number range noted above. A number of observations can be made. There are only two symmetric hairpin vortices in figures 12(i) and 12(ii) (marked HP). As noted earlier, symmetric hairpin vortices are not too common in oscillating flows. Figures 12(ii) and 12(iii) show that some structures are heterostrophic vortex pairs (labelled HsV). All structures are not vortices or do not look like vortices. Figures 13(i)–13(iii) show the flow features in a vertical light plane intersecting the horizontal cylinder at a 45° angle. Figure 13(i) shows the inception of the streaks and figures 13(ii)–13(iv) show randomly selected close-up views of the vortical structures (each closer than the previous one). Vortex pairs can be distinguished and in some cases compared with those in the (z, x)-plane. Evidently, all vortical structures are not in the transverse direction ((r, θ)-plane) and the vortical structures which are in the transverse direction span only over a short distance. The most vivid perception of the evolution of the vortical structures can be acquired only from seeing them move across the 45° light plane. Unfortunately, the sensation of such a motion cannot be conveyed through two-dimensional still pictures.

At higher values of Re_δ (~ 600), transitional activity spanned over larger times and larger areas. The number and the speed of occurrence of the structures increased. Figures 14(i) and 14(iii) show numerous structures (some are clearly vortical) near the end of the deceleration period. Figure 14(iv), an enlargement of one of the structures from another frame, shows that vortex pairs (probably inclined to the streamwise direction) still dominate the flow. At still higher values of Re_δ (~ 800), identification

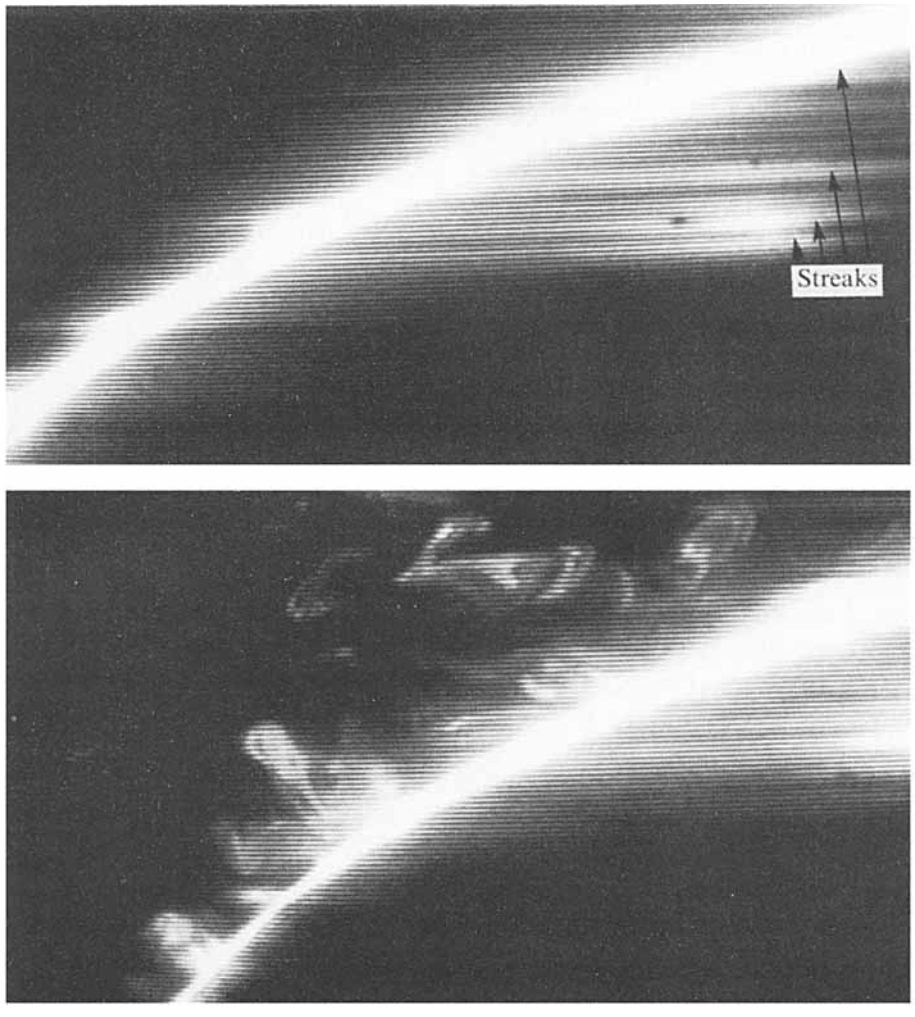

FIGURE 13(i, ii). For caption see facing page.

of structures (with the instruments available) during the deceleration period becomes difficult as turbulence covers an ever increasing range of scales. During the acceleration phase, however, particularly for Re_δ smaller than about 1000, turbulence is essentially the vestiges of more energetic structures which came into existence by violent bursting during the deceleration phase.

As Re_δ was increased further, turbulent motion prevailed over larger fractions of the flow cycle, both during the deceleration and the acceleration phase. However, even at Re_δ as large as 1800, there were still some time intervals in the cycle where the flow was either in a transitional or partially developed turbulent state.

It would have been most desirable to have views of the quasi-coherent structures in all planes (see figure 3) to simplify and enhance the correlation between them. However, unlike the experiments with synthetic hairpins (see e.g. Acarlar & Smith 1987), the flow structures in an oscillating flow look more irregular and do not necessarily repeat themselves in the same volume of observation. Thus, it is nearly impossible to produce contemporary views of a given structure in all possible planes. This is one of many difficulties encountered in the study of natural transition in non-canonical flows.

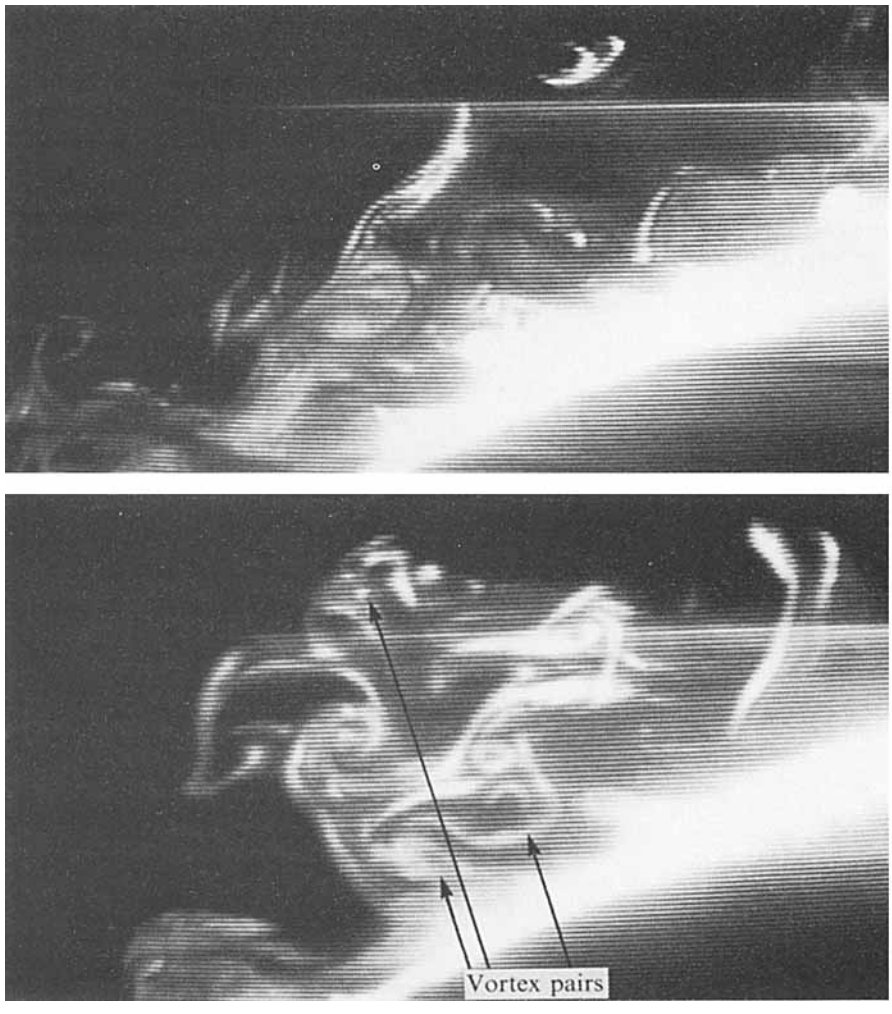

FIGURE 13. The vortical structures in a vertical light plane intersecting the horizontal cylinder at a 45° angle. (i) shows the inception of the streaks and (ii)–(iv) show randomly-selected close-up views of the vortical structures (each closer than the previous one). Vortex pairs can be distinguished (in iv) and in some cases compared with those in the (z, x)-plane (in figure 12iv).

3.3. *Streak response to change in wall shear*

A series of exploratory experiments were carried out to ascertain the effect of artificially increasing or decreasing the wall shear in the area of observation in order to understand how the change in physical characteristics of a thin layer alters the structure of turbulence nearby. For this purpose glycerol (10% by weight) and a small amount of fluorescein were mixed in one litre of water and strained. At 20 °C (temperature of the tunnel water), the specific gravity of the solution is 1.024 and its kinematic viscosity is about 35% larger than that of water (Hodgman 1963). Brine was added into the tunnel to increase the specific gravity of water to 1.023. Then about 30 cm^3 dye solution was remotely applied over an area (15 cm wide, 40 cm long) near the top of the cylinder, in order to achieve a dye layer of about 10 wall units thick (about 0.5 mm). The dye layer was made intentionally thick in order to account for the spreading and diffusion of the layer during the transient period of the oscillations

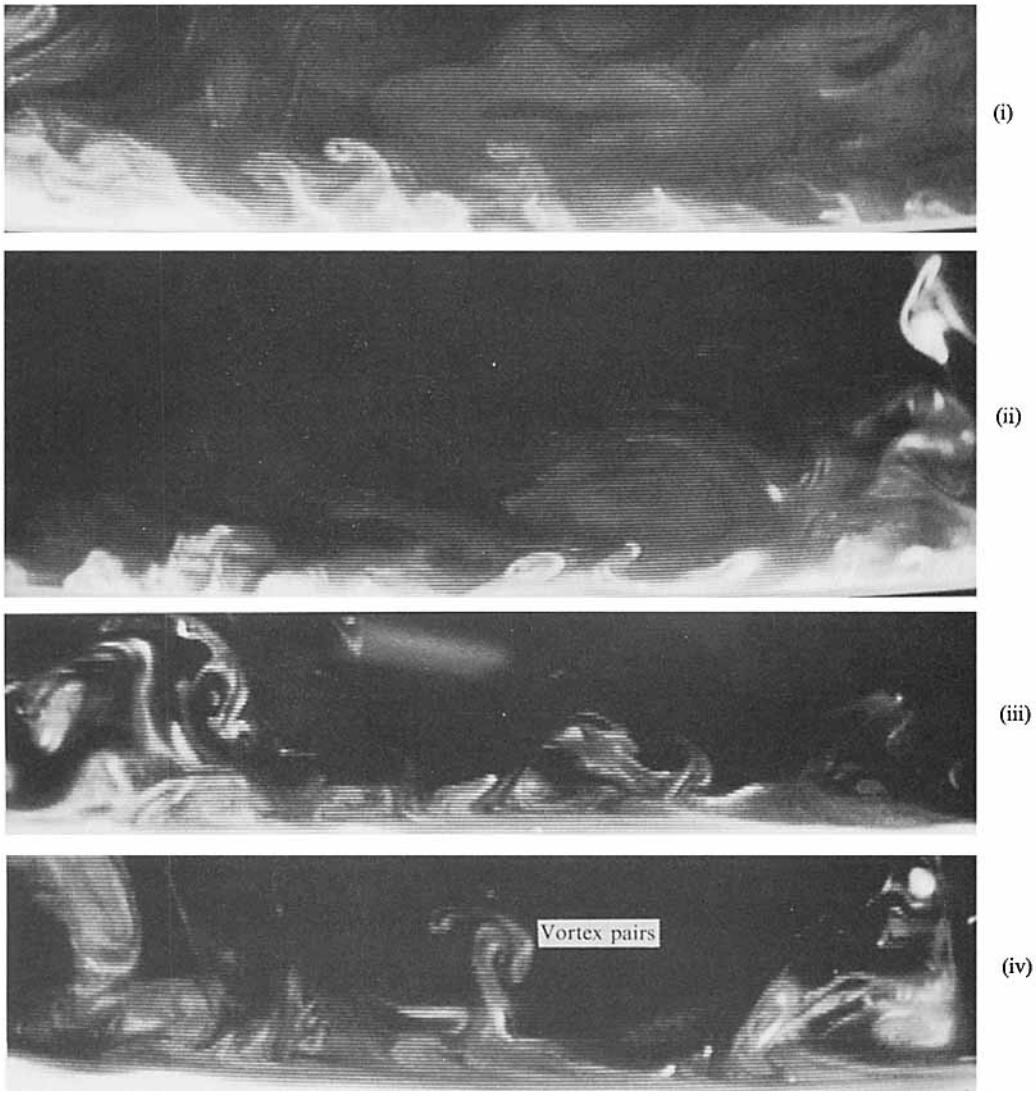

FIGURE 14. Numerous quasi-coherent structures near the end of the deceleration period. (iv) An enlargement of one of the structures from another frame, shows that vortex pairs (probably inclined to the streamwise direction) still dominate the flow.

(about seven cycles). The final thickness of the solution at the time of occurrence of the streaks is estimated to be about 6 wu, with an intermediate layer of transitional viscosity above it.

It can be shown theoretically that in a two-layer oscillatory Stokes flow of uniform density, subjected to a sinusoidal pressure gradient (of amplitude $= \rho\omega U_{\max}$), v^* on the wall can be increased or decreased by making the viscosity of the layer adjacent to the wall higher or lower than that of the upper layer. Of course the analysis assumes that the two layers maintain a stable sharp viscosity interface and extend to infinity in the horizontal direction. There is an extensive literature on the analysis of the instability of a liquid/liquid interface (see e.g. Oliemans & Ooms 1986; Hooper & Boyd 1987; Miesen *et al.* 1992). The growth rate of the instability is determined by the ratio of the viscosities and densities of the two fluids and the depth of the lower bounded fluid.

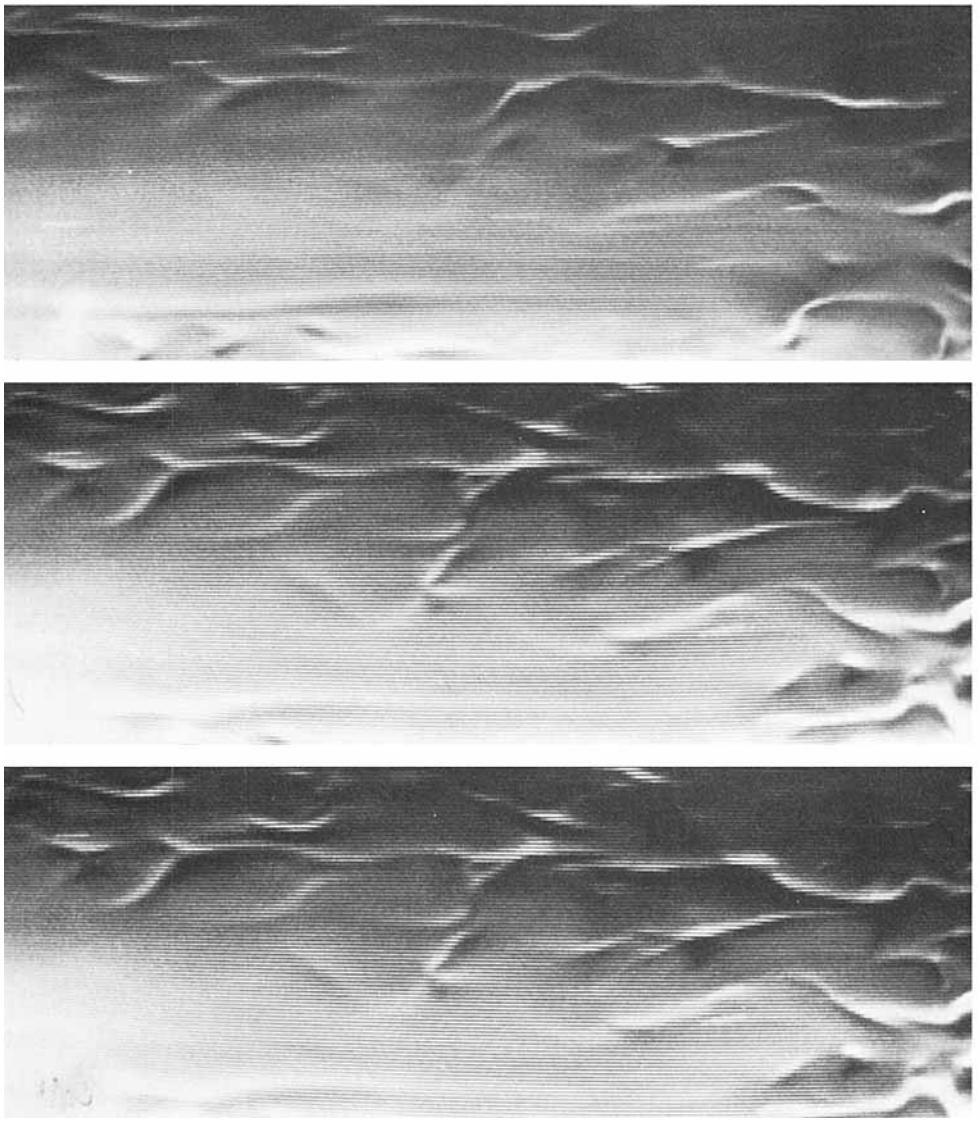

FIGURE 15(i–iii). For caption see p. 135.

There are three main types of instability for fluids of equal density: (i) the Yih-type (1967) long-wave instability if the lower bounded fluid is more viscous than the upper unbounded fluid; (ii) the short-wave instability which occurs solely because of the presence of the interface; and (iii) the Hooper–Boyd-type (1987) instability which arises at the viscous boundary layer at the wall and is only apparent when the kinematic viscosity of the lower bounded fluid is less than the kinematic viscosity of the upper unbounded fluid. In the present exploratory experiments, the fluid with larger viscosity is spread only over a small portion of the cylinder surface and the flow is considerably more complex. Nevertheless, the observations are thought to be instructive in understanding the behaviour of streaks since 'the wall indirectly assists in the maintenance of mean velocity gradients which in turn interact with the turbulent fluctuations to produce new turbulence' (Uzkan & Reynolds 1967).

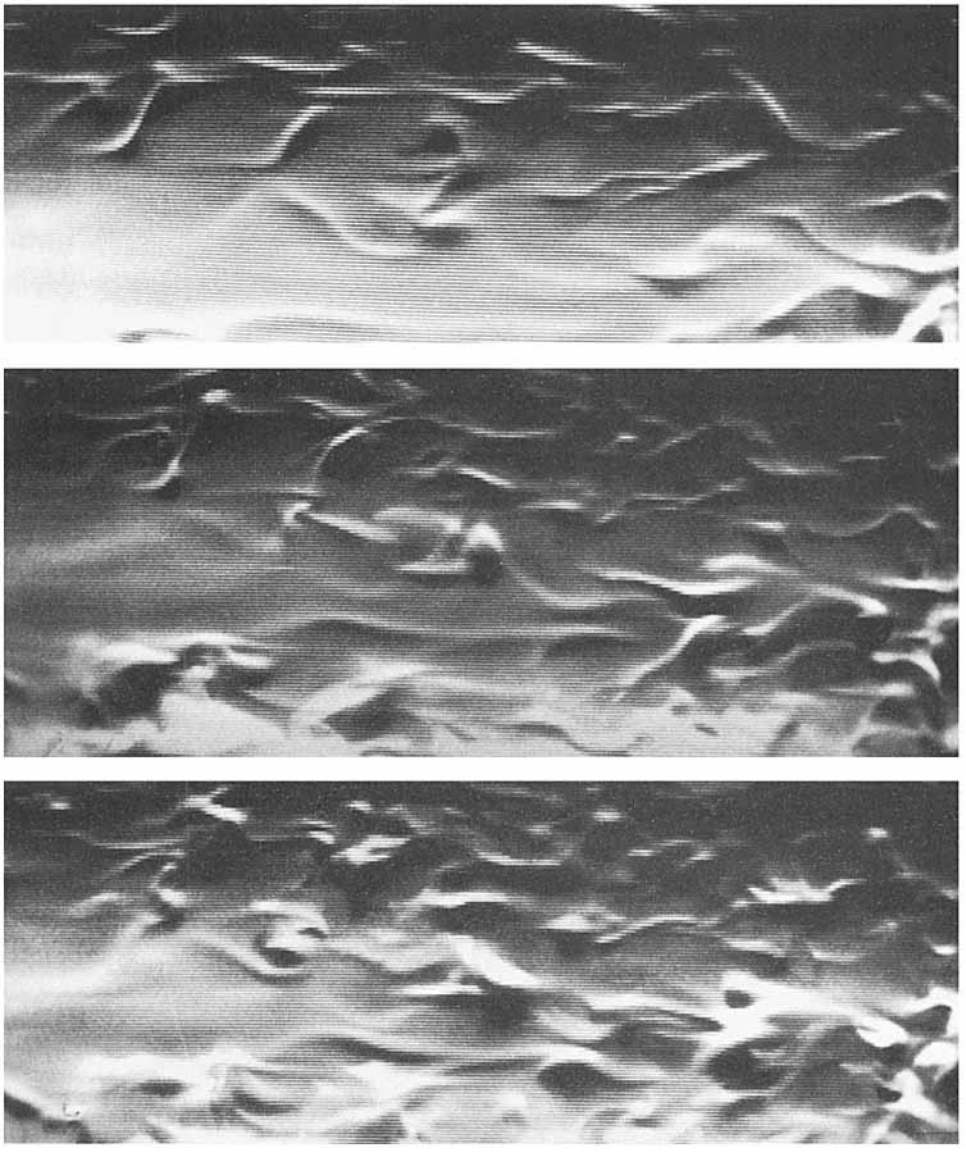

FIGURE 15(iv–vi). For caption see facing page.

The flow was set to oscillate at a Reynolds number of Re_δ(wall) $\approx$ 460 (based on the dye-solution viscosity) or at Re_δ(water) $\approx$ 525 (based on outer flow viscosity, note that $Re_\delta \propto \nu^{-\frac{1}{2}}$). The resulting streak formation, which began at about -113 tu (based on outer flow properties) is shown in figures 15(i)–15(x) (12.5 tu apart). The structural differences in streak formation relative to the pure water case are rather striking. A large number of streaks came into existence almost simultaneously (the flow is from right to left) and began to bifurcate rapidly. The initial bifurcations were at angles of about 45°. At larger times (i.e. after about 0.15 s), the angle of bifurcation and the average streak spacing decreased rapidly. The size and number of the streaks increased and the entire surface became turbulent in about half the time period compared with the pure water case (see figures 7i–7xx). Even the qualitative nature of the turbulent

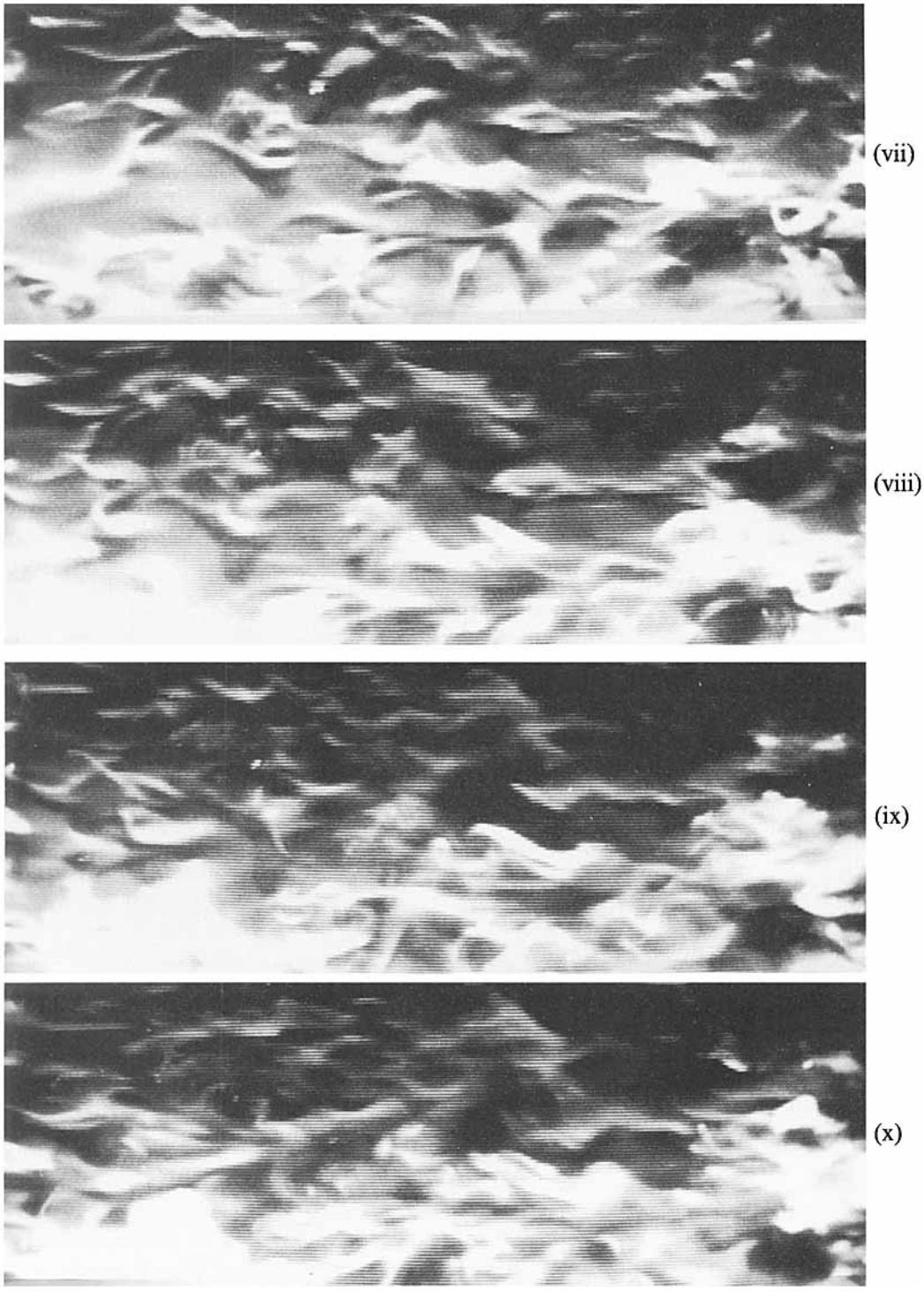

FIGURE 15. The evolution of low-speed streaks when the viscosity of the fluid in the wall layer is increased by about 30% (the first frame is at about -113 time units from the moment of maximum deceleration. Subsequent frames are 12.5 time units apart). The structural differences in streak formation relative to the pure water case (see figures 7i–7xxv) are rather striking.

structures was different, i.e. the higher-viscosity wall layer appeared to increase the production of turbulence. It is reasonable to assume that the spanwise gradients (in the θ-direction) are considerably larger than those for the pure water case due to bifurcations. These effects were brought about by manipulating one of the physical properties of the fluid in the near-wall region. Available evidence tends to support the above observations. Rashidi & Banerjee (1990) and Lam & Banerjee (1992) have shown through physical and numerical experiments that the streaks become more pronounced if the shear is increased near the wall and vice versa. Uzkan and Reynolds (1967) have shown that, in the absence of mean velocity gradients, the wall acts to attenuate the turbulence, emphasizing the importance of shear rate alone. Finally, even though more complex and somewhat further removed from our objectives, the flow-visualization study of Donohue, Tiederman & Reischman (1972) on the near-wall region in a drag-reducing channel flow has shown that the dilute polymer solution decreases the production of turbulent kinetic energy by inhibiting the formation of low-speed streaks. The preliminary results of our ongoing work with a suitably prepared aqueous methyl alcohol solution (whose kinematic viscosity was about 20% smaller than that of water) have shown that the streak formation in the wall-bounded fluid decreases, average streak spacing (about 150 wu) is greater than that in pure water, and streaks are cleaner, smoother, straighter and sharper relative to those shown in figures 7 and 8. The streaks had no tendency to bifurcate but did eventually break up as the flow neared the end of its deceleration phase. The burst events did not appear to be as violent as the pure water case. The results regarding the manipulation of the viscosity of the wall-layer fluid are based on a limited range of experiments and must be regarded as somewhat tentative at this time.

4. Concluding remarks

The circumstances leading to the creation and subsequent evolution of low-speed streaks and other quasi-coherent structures on a long cylindrical body immersed in a sinusoidally oscillating flow were investigated experimentally in a U-shaped water tunnel. The flow field was visualized using fluorescent dyes and sheets of argon laser light. The wall shear stress and the phase lead of the maximum wall shear over the maximum free-stream velocity were measured to characterize the unsteady boundary layer.

The oscillatory nature of the flow allowed the observation of the entire life cycle of a limited number of low-speed streaks and other turbulence structures. Comparisons can be made judiciously with other results from the literature for oscillatory flows and with results from steady canonical transitional and turbulent flows (numerical and experimental) without implying that the mechanisms causing the events in oscillatory and steady flows are the same.

The transition to turbulence in oscillatory Stokes flow is a gradual quasi-deterministic process. It has a beginning (when it is large enough to be seen), a reasonably clear intermediate step (when it exhibits a dramatic change in one or more measurable parameters), and no discernible end. For $Re_\delta \approx 400$, one or more unevenly spaced low-speed streaks emerge toward the end of the deceleration phase and then completely disappear during the acceleration phase, without ever giving rise to any coherent structures. In the range of $Re_\delta \approx 420$–460, the vortical structures begin to emerge and continue to increase in number, over larger time intervals. The next major change occurs in the narrow interval of Re_δ values from about 780 to 880 in which the phase angle decreases sharply from about 34° to about 13° and the friction coefficient

increases rapidly and reaches a local maximum at about $Re_\delta \approx 1000$. At these Reynolds numbers, turbulence is essentially the vestiges of more energetic structures which come into existence by violent bursting during the deceleration phase, as evidenced by extensive viewing of video tapes.

The transitional and turbulent states in oscillatory Stokes flow exhibit very few symmetric hairpin vortices, fewer than that seen and described by Head & Bandyopadhyay (1981) and certainly fewer than that required by Smith *et al.* (1991) for their streak-generation model in canonical flows. It seems that the emergence of coherent structures during a relatively brief period (in the later stages of the deceleration phase) and the premature termination of their growth by the reversal of flow are primarily responsible for the infrequent occurrence of hairpin vortices in oscillating flow. Also, it seems that the form and frequency of the hairpins are dependent not only upon the Reynolds number but also on the characteristics of the imposed unsteadiness. While the hairpins in steady boundary layers with zero pressure gradient are 'arrayed at a characteristic angle of approximately 45° to the wall' (Head & Bandyopadhyay 1981), in our oscillatory flow no characteristic angle was discernible, i.e. the hairpins may be arrayed at almost any angle. However, as in steady flow, the tips of the hairpins are inclined forward into the flow. The birth of one or more streaks at $Re_\delta \approx 400$ is not accompanied by hairpin vortices. Had they existed, the flow visualization employed herein could not have failed to reveal their existence. This does not, however, mean that hairpin vortices, once existent, cannot give rise to new short streaks. Nevertheless, it is difficult to accept that the hairpin vortices, which we have rarely seen, or the 'typical eddies', which we have never seen (nor are we willing to assume that they represent the longitudinal sections of the tips of hairpin vortices) can account for the observations we have made.

In Kim *et al.*'s (1971) scenario, the inflexional velocity profiles are created instantaneously by low-speed streaks slowly moving away from the wall. This results in oscillatory motions that quickly lead to quasi-coherent structures and turbulence production. Thus, it is natural to assume that if one or more streaks came into existence in an oscillating flow, where the inflexion points occur naturally, one would expect the onset of oscillatory motions which would quickly lead to the creation of quasi-coherent structures. Our experiments near $Re_\delta = 400$ have shown conclusively that streaks and inflexion points (at least during part of the cycle) can co-exist indefinitely without ever leading to quasi-coherent structures. Thus, the Reynolds number must exceed a critical value (Re_δ(min) ≈ 420) for the oscillatory motions to give rise to quasi-coherent structures. This is in conformity with the conclusions of some of the numerical simulations. Lee, Kim & Moin (1990) found that high shear rate alone is sufficient for generation of the streaky structures, and that the presence of a solid boundary is not necessary. Lam & Banerjee (1992) concluded, on the basis of their numerical simulations of a channel flow, that there is a critical value of the shear Reynolds number $Re^* = v^*\delta/\nu, \{= (\sqrt{2}\, Re_\delta)^{\frac{1}{2}}\}$, at which the wall-layer streaks disappear. Their suggested value for Re^*(crit) ranged from 20 to 28. The use of an average value of Re^*(crit) ≈ 24 yields $Re_\delta \approx 400$, the Reynolds number at which the streaks appeared and disappeared periodically in our experiments. This unexpected agreement should be regarded as fortuitous since the two flows have very different characteristics.

It is hoped that the present study of the evolution of quasi-coherent structures, in a flow rich with a variety of characteristics including strong adverse pressure gradients, inflexion points, shear reversal, phase locked transition, and fossil vorticity, raised serious questions about a number of basic tenets in our perception of the nature of turbulent boundary layers. In the context of the present paper, the non-canonical flows

may provide clearer insight into the physics of the turbulent processes as well as the direct numerical simulation of turbulent wall flows.

This research has been supported by the National Science Foundation and the Office of Naval Research. The constructive comments of Professor F. K. Browand and the reviewers are sincerely appreciated. Thanks are also due to Messrs. M. Cady, R. Hooper, and J. McKay for their assistance with the experiments.

REFERENCES

ACARLAR, M. S. & SMITH, C. R. 1987 A study of hairpin vortices in a laminar boundary layer. Part 2. Hairpin vortices generated by fluid injection. *J. Fluid Mech.* **175**, 43–83.

BLACKWELDER, R. F. & ECKELMANN, H. 1979 Streamwise vortices associated with the bursting phenomenon. *J. Fluid Mech.* **94**, 577–594.

CASARELLA, M. J. & LAURA, P. A. 1969 Drag on an oscillating rod with longitudinal and torsional motion. *J. Hydronautics* **3**(4), 180–183.

CHEW, Y. T. & LIU, C. Y. 1988 Effects of transverse curvature on oscillatory flow along a circular cylinder. *AIAA J.* **27**, 1137–1139.

COLLINS, J. I. 1963 Inception of turbulence at the bed under periodic gravity waves. *J. Geophys. Res.* **68**, 6007–6014.

CORINO, E. R. & BRODKEY, R. S. 1969 A visual investigation of the wall region in turbulent flow. *J. Fluid Mech.* **37**, 1–30.

COUSTEIX, J., HOUDEVILLE, R. & JAVELLE, J. 1981 Response of a turbulent boundary layer to a pulsation of the external flow with and without adverse pressure gradient. In *Unsteady Turbulent Shear Flows* (ed. R. Michel, J. Cousteix & R. Houdeville), pp. 120–139. Springer.

COWLEY, S. J. 1987 High frequency Rayleigh instability of Stokes layers. In *Stability of Time Dependent and Spatially Varying Flows* (ed. D. L. Dwoyer & M. Y. Hussaini), pp. 261–275. Springer.

DONOHUE, G. L., TIEDERMAN, W. G. & REISCHMAN, M. M. 1972 Flow visualization of the near-wall region in a drag-reducing channel flow. *J. Fluid Mech.* **56**, 559–575.

ECKMANN, D. M. & GROTBERG, J. B. 1991 Experiments on transition to turbulence in oscillatory pipe flow. *J. Fluid Mech.* **222**, 329–350.

FALCO, R. E. 1991 A coherent structure model of the turbulent boundary layer and its ability to predict Reynolds number dependence. *Phil. Trans. R. Soc. Lond.* A **336**, 103–129.

FISHLER, L. S. & BRODKEY, R. S. 1991 Transition, turbulence and oscillating flow in a pipe – a visual study. *Exps Fluids* **11**, 388–398.

HALL, P. 1978 The Linear stability of flat Stokes layers. *R. Soc. Lond.* A **359**, 151–166.

HAYASHI, T. & OHASHI, M. 1982 A dynamical and visual study on the oscillatory turbulent boundary layer. In *Turbulent Shear Flows 3* (ed. L. J. S. Bradbury, F. Durst, B. E. Launder, F. W. Schmidt & J. W. Whitelaw), pp. 18–33. Springer.

HEAD, M. R. & BANDYOPADHYAY, P. 1981 New aspects of turbulent boundary layer structure. *J. Fluid Mech.* **107**, 297–338.

HINO, M., KASHIWAYANAGI, M., NAKAYAMA, A. & HARA, T. 1983 Experiments on the turbulence statistics and the structure of a reciprocating oscillatory flow. *J. Fluid Mech.* **131**, 363–399.

HINO, M., SAWAMOTO, M. & TAKASU, S. 1976 Experiments on transition to turbulence in oscillatory pipe flow. *J. Fluid Mech.* **75**, 193–207.

HODGMAN, C. D. (ed.) 1963 *Handbook of Chemistry and Physics*, p. 2273. Cleveland: The Chemical Rubber Publishing Co.

HOOPER, A. P. & BOYD, W. G. C. 1987 Shear-flow instability due to a wall and viscosity discontinuity at the interface. *J. Fluid Mech.* **179**, 201–225.

JENSEN, B. L., SUMER, B. M. & FREDSOE, J. 1989 Turbulent oscillatory boundary layers at high Reynolds numbers. *J. Fluid Mech.* **206**, 265–297.

JIMENEZ, J. & MOIN, P. 1991 The minimal flow unit in near-wall turbulence. *J. Fluid Mech.* **225**, 213–240.

KAMPHUIS, J. W. 1975 Friction factor under oscillatory waves. *J. Waterways, Port Coastal Engng Div. ASCE* **101**, 135–144.

VON KERCZEK, C. & DAVIS, S. H. 1974 Linear stability theory of oscillatory Stokes layers. *J. Fluid Mech.* **62**, 753–773.

KIM, H. T., KLINE, S. J. & REYNOLDS, W. C. 1971 The production of turbulence near a smooth wall in a turbulent boundary layer. *J. Fluid Mech.* **50**, 133–160.

KIM, J. & MOIN, P. 1986 The structure of the vorticity field in turbulent channel flow. Part 2. Study of ensemble-averaged fields. *J. Fluid Mech.* **162**, 339–363.

KLINE, S. J., REYNOLDS, W. C., SCHRAUB, F. A. & RUNSTADLER, P. W. 1967 The structure of turbulent boundary layers. *J. Fluid Mech.* **30**, 741–773.

KOGA, D. J., ABRAHAMSON, S. D. & EATON, J. K. 1987 Development of a portable laser sheet. *Exps Fluids* **5**, 215–216.

KURZWEG, U. H., LINDGREN, E. R. & LOTHROP, B. 1989 Onset of turbulence in oscillating flow at low Womersley number. *Phys. Fluids* A **1**(12), 1972–1975.

LAM, K. & BANERJEE, S. 1992 On the condition of streak formation in a bounded turbulent flow. *Phys. Fluids* A **4**(2), 306–320.

LANDAHL, M. T. 1990 On sublayer streaks. *J. Fluid Mech.* **212**, 593–614.

LEE, M. J., KIM, J. & MOIN, P. 1990 Structure of turbulence at high shear rate. *J. Fluid Mech.* **216**, 561–583.

LI, H. 1954 Stability of oscillatory laminar flow along a wall. *Beach Erosion Board, US Army Corps Engrs Tech. Memo* **47**.

LIGHTHILL, M. J. 1954 The response of laminar skin friction and heat transfer to fluctuations in the stream velocity. *Proc. R. Soc. Lond.* A **224**, 1–23.

LUEPTOW, R. M. 1990 Turbulent boundary layer on a cylinder in axial flow. *AIAA J.* **28**(10), 1705–1706.

MANKBADI, R. R. & LIU, J. T. C. 1992 Near-wall response in turbulent shear flows subjected to imposed unsteadiness. *J. Fluid Mech.* **238**, 55–71.

MERKLI, P. & THOMANN, H. 1975 Transition to turbulence in oscillatory pipe flow. *J. Fluid Mech.* **68**, 567–575.

MIESEN, R., BEIJNON, G., DUIJVESTIJN, P. E. M., OLIEMANS, R. V. A. & VERHEGGEN, T. 1992 Interfacial waves in core-annular flow. *J. Fluid Mech.* **238**, 97–117.

MONKEWITZ, M. A. 1983 Lineare stabilitätsuntersuchungen an den oszillierenden grenzschichten von Stokes. PhD thesis no. 7297, Federal Institute of Technology, Zurich, Switzerland.

MONKEWITZ, P. A. & BUNSTER, A. 1987 The stability of the Stokes layers: visual observations and some theoretical considerations. In *Stability of Time Dependent and Spatially Varying Flows* (ed. D. L. Dwoyer & M. Y. Hussaini), pp. 244–260. Springer.

NYCHAS, S. G., HERSHEY, H. C. & BRODKEY, R. S. A. 1973 Visual study of turbulent shear flow. *J. Fluid Mech.* **61**, 513–540.

OHMI, M., IGUCHI, M., KAKEHACHI, K. & MASUDA, T. 1982 Transition to turbulence and velocity distribution in an oscillating pipe flow. *Bull. JSME* **25**, 365–371.

OLIEMANS, R. V. A. & OOMS, G. 1986 Core–annular flow of oil and water through a pipeline. In *Multiphase Science and Technology* (ed. G. F. Hewitt, J. M. Delhaya & N. Zuber), vol. 2, chap. 6. Hemisphere.

PANTON, R. L. 1984 *Incompressible flow*. John Wiley & Sons.

PERRY, A. E., LIM, T. T. & TEH, E. W. 1981 A visual study of turbulent spots. *J. Fluid Mech.* **104**, 387–405.

RAMAPRIAN, B. R. 1984 A review of experiments in periodic turbulent pipe flow. In *Unsteady Turbulent Boundary Layers and Friction, ASME*, **FED-12**, 1–16.

RAMAPRIAN, B. R. & TU, S. W. 1983 Fully developed periodic turbulent pipe flow. Part 2. The detailed structure of the flow. *J. Fluid Mech.* **137**, 59–113.

RASHIDI, M. & BANERJEE, S. 1990 The effect of boundary conditions and shear rate on streak formation and breakdown in turbulent channel flows. *Phys. Fluids* A **2**(10), 1827–1838.

ROBINSON, S. K. 1991 Coherent motions in the turbulent boundary layer. *Ann. Rev. Fluid Mech.* **23**, 601–639. (See also, *NASA Tech. Mem.* 103859, 1991).

ROBINSON, S. K. & KLINE, S. J. 1990 Turbulent boundary layer structure: progress, status and challenges. In *Structure of Turbulence and Drag Reduction* (ed. A. Gyr), pp. 3–32. Springer.

SANDHAM, N. D. & KLEISER, L. 1992 The late stages of transition to turbulence in channel flow. *J. Fluid Mech.* **245**, 319–348.

SARPKAYA, T. 1966 Experimental determination of the critical Reynolds number for pulsating Poiseuille flow. *Trans ASME* D: *J. Basic Engng* **88**, 589–598.

SARPKAYA, T. 1971 On stationary and travelling vortex breakdowns. *J. Fluid Mech.* **45**, 545–559.

SARPKAYA, T. 1976 Vortex shedding and resistance in harmonic flow about smooth and rough circular cylinders at high Reynolds numbers. *Naval Postgraduate School Tech. Rep.* NPS-59SL 76021, Monterey, CA.

SARPKAYA, T. 1978 Hydrodynamic resistance of roughened cylinders in harmonic flow. *J. R. Inst. Naval Arch.* **2**, 41–55.

SARPKAYA, T. 1983 Trailing vortices in homogeneous and density-stratified media. *J. Fluid Mech.* **136**, 85–109.

SARPKAYA, T. 1986*a* In-line and transverse forces on smooth and rough cylinders in oscillatory flow at high Reynolds numbers. *Naval Postgraduate School Tech. Rep.* NPS-69-86-003, Monterey, CA.

SARPKAYA, T. 1986*b* Oscillating flow over bluff bodies in a U-shaped water tunnel. In *Proc. AGARD Symp. on Aerodyn. and Related Hydrodyn. Studies Using Water Facilities*, pp. 6.1–6.15.

SERGEEV, S. I. 1966 Fluid oscillations in pipes at moderate Reynolds numbers. *Fluid Dyn.* **1**, 121–122.

SMITH, C. R., WALKER, J. D. A., HAIDARI, A. H. & SOBRUN, U. 1991 On the dynamics of near-wall turbulence. *Phil. Trans. R. Soc. Lond.* A **336**, 131–175.

SPALART, P. R. & BALDWIN, B. S. 1989 Direct simulation of a turbulent oscillating boundary layer. In *Turbulent Shear Flows* **6**, pp. 417–440. Springer.

TARDU, S. F., BINDER, G. & BLACKWELDER, R. F. 1987 Response of turbulence to large amplitude oscillations in channel flow. In *Advances in Turbulence* (ed. G. Comte-Bellot & J. Mathieu), pp. 546–555. Springer.

UZKAN, T. & REYNOLDS, W. C. 1967 A shear-free turbulent free turbulent boundary layer. *J. Fluid Mech.* **28**, 803–821.

YANG, K.-S., SPALART, P. R. & FERZIGER, J. H. 1992 Numerical studies of natural transition in a decelerating boundary layer. *J. Fluid Mech.* **240**, 433–468.

YIH, C.-S. 1967 Instability due to viscous stratification. *J. Fluid Mech.* **27**, 337–352.